Arabian Journal for Science and Engineering

https://www.springer.com/journal/13369

Impact factor = 2.334

Accepted November 29th, 2021

Convective Flow of Non-Homogeneous Fluid Conveying Nano-Sized Particles with Non-Fourier Thermal Relaxation: Application in Polymer Coating

Atul Kumar Ray[1,2*], B. Vasu[3], P. V. S. N. Murthy[4], O. Anwar Bég[5], R. S. R. Gorla[6] and B. Kumar[7]

[1] Engineering Mathematics and Computing, Madhav Institute of Technology and Science Gwalior- 474005, M.P., India

[2] Centre for Applied Mathematics and Computing, ITER, Siksha 'O' Anusandhan, Bhubaneswar- 751030, Odisha, India

[3] Department of Mathematics, Motilal Nehru National Institute of Technology, Allahabad, Prayagraj-211004, India

[4]Department of Mathematics, Indian Institute of Technology, Kharagpur 721302, India

[5]Multi-Physical Engineering Sciences Group, Aeronautical/Mechanical Engineering, Salford University, M54WT, UK

[6]Department of Aeronautics and Astronautics, Air force Institute of Technology, Wright Patterson Air Force Base, Dayton, Ohio, USA

[7]School of Mathematics, Thapar Institute of Engineering and Technology, Patiyala-147004, Punjab, India

*Corresponding Author Email: akray18490@gmail.com

ABSTRACT

The present article addresses the steady incompressible convective flow of kinetic theory-based Eyring-Powell fluid conveying nano-sized particle from a vertical plate with convective boundary condition and distribution of nanoparticles fraction over its surface. Cattaneo-Christov model is imposed to scrutinize the heat transfer analysis. A revised Buongiorno nanoscale model is adopted, which considers zero nanoparticle flux at the wall surface and simulates physically more viable scenarios for nanoparticle distribution. The study has applications in designing heat exchangers, cooling metallic plates, surface coating dynamics etc. The reduced non-linear equations in (η, ξ) coordinate system transformed from (x, y) coordinate system is non-similar nature and are solved by using two efficient techniques: the Sparrow-Yu local non-similarity method and the Liao Homotopy Analysis Method (HAM). Excellent corroboration of the converged results for both methods is achieved with the existing results. In order to discuss the influence of thermophysical parameters, the HAM simulations have been presented graphically and tabulated to visualize the distribution of skin friction coefficient, rate of heat transfer (Nusselt number) and mass transfer rate (Sherwood number) for the boundary layer regime. It is observed that the Eyring-Powell fluid conveying nano-sized particle attains a higher velocity but lower

temperatures than Newtonian fluid conveying nano-sized particle. The presence of radiative heat flux remarkably increases the magnitudes of temperature. Skin friction factor exhibits an inverse relation with Deborah (viscoelastic) number and Cattaneo-Christov thermal relaxation parameter. Nusselt number increases whereas nanoparticle Sherwood number decreases with increment in Eyring-Powell parameter and mixed convection parameter. The current simulations furnish interesting insights into non-Newtonian nano-coating dynamics of relevance in the polymer processing industry.

Keywords: *Mixed convection; Eyring-Powell fluid conveying nano-sized particle; non-Fourier thermal relaxation; Revised Buongiorno nanofluid model; Convective boundary condition; Homotopy analysis method.*

1. INTRODUCTION

Convective heat and mass transfer phenomena in non-Newtonians from a vertical surface emerge in many diverse technologies including composite processing, energy systems, nuclear reactor design, thermal ducts, polymer devolatilization and coating of aerospace and marine components etc. Owing to such applications, many researchers have contributed towards the study of thermal/thermosolutal flow in non-Newtonian fluids along vertical surfaces which have provided a robust compliment to experimental investigations. An extensive range of different rheological formulations have been adopted in such studies which often also feature external boundary layer flows. These include Rajagopal and Na [1] studied the convective flow of non-Newtonian fluid in between two parallelly aligned sheets whereas Huang et al. [2] discussed the natural convection from vertical plate due to the non-Newtonian fluid flow. In continuation of these studies, the mixed convective power-law rheological fluid flow along a porous vertical plate was numerically investigated using a finite difference method (FDM) by Gorla et al. [3]. Gupta et al. [4] implemented a finite element method (FEM) to examine the micropolar convection boundary layer flow from a vertical permeable surface. Rao et al. [5] investigated the hydrodynamic and thermal slip effects on viscoplastic thermal convective flow from a vertical surface with the Casson rheological model and a finite difference code. Bég et al. [6] took use of a network electrothermal solver (PSPICE) to imitate transient free convection of a Walters-B liquid from a vertical sheet in Darcy-Forchheimer permeable media. Bég and Makinde [7] employed MAPLE shooting quadrature and a Maxwell upper convected model to investigate the mass diffusion in porous media along vertical walls of a channel. Ray et al. [8] used the HAM to derive non-similar solutions for convective flow of Eyring-Powell fluid from a convectively heated vertical plate. Manghat et al. [9]

discussed the two-phase Sakiadis flow of a nanoliquid with nonlinear Boussinesq approximation and Brownian motion past a vertical plate.

The characteristics of heat transfer can be increased by raising the thermal conductivity of base fluid like engine oil, water and ethyl glycol etc. The thermal conductivity of solids is more than liquids so suspending nano-sized solid particles in the base fluid results in enhancing the thermal conductivity of the resultant colloidal suspension, which is termed a nanofluid. Fluid conveying nano-sized particle have found significant applications in coating systems, thermal ducts, biomedical sciences, nuclear reactors, heat exchanger and cooling of electrical devices. Fundamentally two mathematical models have become popular for describing the transport phenomena in nanofluids and these are homogeneous and non-homogeneous nanofluid models. The homogeneous model, also known as the single-component model provides a correlation between thermophysical properties of base fluid (viscosity, density, thermal conductivity) and nanoparticle thermal conductivity. The homogeneous model ignores the nanoparticle's slip mechanism. The two-component (non-homogeneous) model is considerably more complex. It features seven mechanical mechanisms considered by Buongiorno [10] i. e. gravity, inertia, fluid drainage, Magnus effect, thermophoresis, Brownian motion and diffusiophoresis. Out of these slip mechanisms, thermophoresis and Brownian motion [11] are emphasized in the Buongiorno non-homogeneous two-component model. The Buongiorno model for nanofluid transport was modified and the revised model more accurately accounts for the impact of nanoparticle distribution [12-13] i. e. correctly considers zero nanoparticle flux at the wall surface and achieves more practical results. Many researchers have implemented the modified Buongiorno model for different problems in nanofluid transport. Malvandi and Ganji [14] discussed the influence of Brownian motion and thermophoresis on the flow of Al_2O_3/water nanofluid inside a circular microchannel using revised Buongiorno model. In a recent meta-analysis on the transport phenomenon of various nanofluids, it was concluded that increasing haphazard motion of tiny/nano-sized particles is capable to cause an increase in the internal pressure on the tinyparticles [15]. Another meta-analysis by Wakif et a. [16] on the effects of thermophoresis shows that different responses to the force of a temperature gradient are sufficient enough to enhance the temperature distribution due to an increase in thermophoresis. Ray et al. [17] used modified Buongiorno model to investigate the flow of Power-law fluid past multiple geometries. Vasu et al. [18] implemented a FREEFEM++technique to compute the two-dimensional magneto-hemodynamic nanoparticle-doped blood flow through stenosed coronary artery with the modified Buongiorno model.

In a variety of industrial systems, the conventional Fourier heat conduction model [19] is inadequate. This conventional model displays infinitesimal heat disturbance which generate at a very high speed since it contradicts the principle of casualty with a parabolic nature, whereas thermal

relaxation produces a hyperbolic behaviour [20]. Cattaneo's model however does not preserve the property of invariance. Christov [21] later therefore altered the Cattaneo model by restoring the derivative term with an Oldroyd formulation which overcomes the problem of invariance. The Cattaneo-Christov model is a robust revised version of the classical Fourier-law. It has been formulated such that the principle of casualty can be avoid and to preserve invariance. The Oldroyd derivative is used in Cattaneo-Christov heat flux model which contains thermal relaxation time and results in thermal relaxation parameter in the reduced equation. Thus the non-Fourier thermal relation parameter denotes the thermal relaxation parameter corresponding to Cattaneo-Christov heat flux model**.** Reddy et al. [22] scrutinized the impact of cross diffusion and thermal relaxation on external boundary layer flows for different geometries with Cattaneo-Christov flux. Shahid et al. [22] deployed a Taylor successive approximation method to compute the non-Fourier convection flow of an electroconductive rheological Maxwell fluid from a stretching permeable sheet with radiative heat flux effects. Sarkar and Kundu [23] computed the Cattaneo-Christov flux effects on the flow of viscoelastic nanofluid with heterogeneous/homogeneous reactions. Vasu et al. [24] emphasized the significance of the convective boundary condition on thermally stratified viscous flow with thermal dispersion numerically by considering thermodynamic optimization with Bejan's method. Akbar et al. [25] implemented a Runge-Kutta method to compute the MHD nanofluid Sakiadis flow with a non-Fourier model and revised Buongiorno nanoscale model. They showed that temperature is boosted with higher Brownian motion parameter. Vasu et al. [26] applied Cattaneo-Christov model in order to analyse convective Jeffrey viscoelastic nanofluid flow (considering relaxation and retardation effects in the rheology) along a vertical sheet. Mehmood et al. [27] investigated the reactive hydromagnetic non-orthogonal stagnation flow of an Oldroyd-B polymeric coating on a horizontal substrate with a non-Fourier model for nuclear reactor wall thermal protection. They observed that wall heat transfer rate and wall species transfer rate are reduced with non-Fourier effect increased with greater effect of heterogeneous reactions whereas they are suppressed with greater effect of homogeneous reactions. Vasu and Ray [28] deployed both local non-similarity and homotopy analysis methods to compute the transport phenomena in nanofluid flow from a vertical surface with the Cattaneo–Christov and Buongiorno nanoscale models.

As noted earlier, there is presently no generic constitutive equation that can robustly simulate all the diverse characteristics of non-Newtonian fluids. Different phenomena e. g. thixotropy, stress relaxation, stress retardation, secondary stresses, memory etc, require different rheological models, many of which are lucidly reviewed in the excellent treatises of Irgens [29] and Chhabra and Richardson [30]. These non-Newtonian models feature varying degrees of non-linearity and different derivative types. The extensive variety of coatings deployed in industry requires different rheological models to capture

their shear stress strain behaviour correctly. Interesting models which have been utilized in recent years in this regard include the Walters-B short memory elastico-viscous model [31], Spriggs four-constant viscoelastic mode for polymer melts (which combines results from molecular theory with continuum mechanics), Dubey et al. [33] (Sisko viscoelastic model), Ali et al. [34] (Giesekus memory fluid) Manzoor et al. [35] (Johnson-Segalman model), Gaffar et al. [36] (tangent hyperbolic model), Kumar et al. [37] (Williamson viscoelastic model), Norouzi et al. [38] (FENE P visco-elastic model), Umavathi and Bég [39] (Stokes' couple stress polar model) Bég et al. [40] (Reynolds exponential viscosity model). In the present study, motivated by developing more sophisticated models for industrial coatings, an alternative non-Newtonian model is utilized. The Eyring-Powell fluid model [41] is a unique non-Newtonian model since it is formulated with the kinetic theory which includes collision of molecules within the fluids. Many technological coatings approximate well to this model. The Eyring-Powell model has therefore been implemented in a number of recent studies. In a study on the dynamics of three-dimensional Eyring-Powell 36 nm alumina-water nanofluid within the thin boundary layer experiencing quartic autocatalytic kind of chemical reaction, it was discovered that increasing thermal stratification indeed cause a decline in the temperature distribution but causes the same temperature gradient associated with not only heat transfer rate but also with thermophoresis to be enhanced significantly near the wall [42]. According to Abegunrin et al. [43], on the surface of upper horizontal surface of a paraboloid of revolution, rapid increase in the temperature distribution due to an increase in the magnitude of one of the Eyring-Powell fluid parameters is guaranteed. Further studies employing the Eyring-Powell fluid model in coating dynamics include Kumaran et al. [44] who used Keller's box finite difference method to simulate variable thermophysical effects on natural axisymmetric hydromagnetic Powell-Eyring nanofluid flow from permeable cylinder. Gaffar et al. [45] investigated the Eyring Powell electromagnetic polymer coating flow from wedge configuration using Keller box and smoothed particle hydrodynamic (SPH) techniques.

To the author's knowledge, no attempt has been done to investigate the non-Fourier convective coating flow on a vertical surface under strong radiative flux with the kinetic theory based Eyring Powell fluid conveying nano-sized particle flow with a revised Buongiorno nanofluid model. The transformed two-dimensional equations are solved by local non-similarity method and Liao homotopy simulation method (HAM). The novelty of this work is therefore to extend the current literature to consider Cattaneo-Christov heat flux, radiative heat flux, modified nanoparticle wall boundary conditions and the Eyring-Powell rheological formulation. Section 2 concerns with the mathematical modeling of the flow problem. Sections 3 and 4 describe the numerical solution procedures with validation to published

studies. Section 5 presents extensive visualization of the LNM/HAM computations with detailed physical interpretation.

2.MATHEMATICAL MODEL FOR NON-NEWTONIAN NANOFLUID COATING FLOW

A two-dimensional mixed convection coating flow of Eyring-Powell fluid conveying nano-sized particle over a vertical surface (substrate) is considered. The vertical wall is prescribed with convective boundary conditions and nano-particle flux at the surface of the plate. The physical configuration is shown in **Fig. 1**. Velocity gradient in the Eyring-Powell fluid conveying nano-sized particle coating flow is very low and hence viscous dissipation is neglected. Also, it is supposed that the nanoparticles do not affect the boundary layer flow problem. Here, the vertical substrate (plate) is parallel to the x -axis and the y -axis is perpendicular to the plate. Velocity component u is orientated along the x direction and v is along the y -axis direction, respectively. C_∞ and T_∞ designate the nanoparticle ambient concentration and ambient temperature.

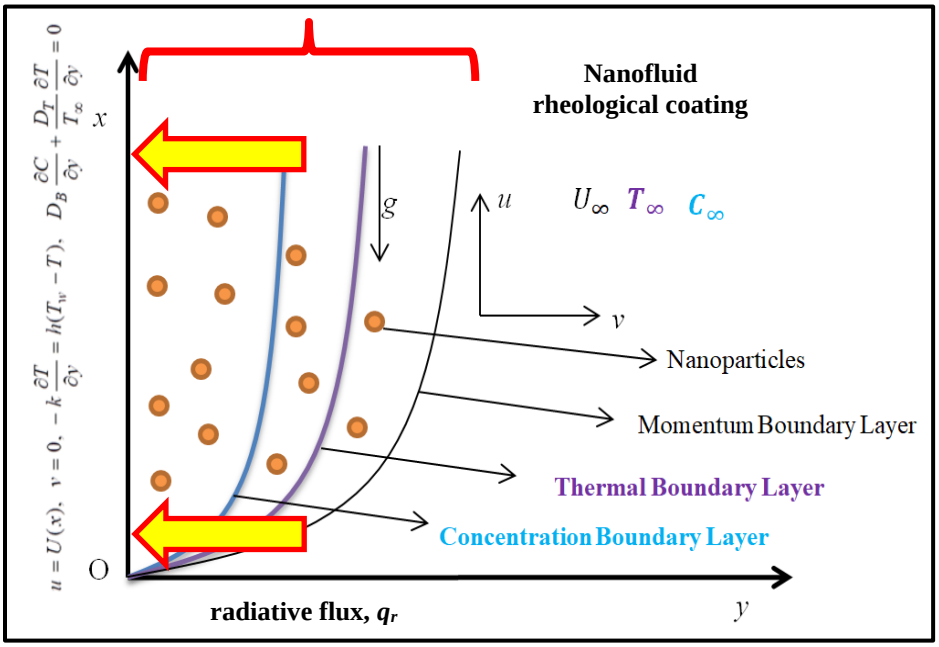

Fig.1. Diagram of coating flow of a vertical substrate

Rosseland's approximation [46] is utilized for radiative heat transfer, such that $q_r = -\frac{4}{3}\frac{\sigma*}{k*}\left(\frac{\partial T^4}{\partial y}\right) = -\frac{16}{3}\frac{\sigma_* T^3}{k*}\left(\frac{\partial T}{\partial y}\right)$, where $\sigma*$ is the Stefan Boltzmann constant and $k*$ is the mean absorption coefficient. The non-Newtonian fluids (*Carreau fluid, power law fluid and Eyring-Powell fluid*) have nonlinear relations between shear stress and shear rate. The non-Newtonian Powell-Eyring constitutive equation

is a complex equation containing three parameters that are generally evaluated by fitting experimental flow data in rheometry [41, 45]:

$$\tau_{ij} = \frac{1}{\beta *}\sinh^{-1}\left(\frac{1}{c}\frac{\partial u}{\partial x}\right) + \mu\frac{\partial u}{\partial x} \tag{1}$$

Here μ is viscosity of the fluid, β ∗, c are constant non-Newtonian fluid material properties. Further first term in RHS of eq. (1) (stress tensor) can be supposed as

$$\sinh^{-1}\left(\frac{1}{c}\frac{\partial u}{\partial x}\right) \cong \frac{1}{c}\frac{\partial u}{\partial x} - \frac{1}{6}\left(\frac{1}{c}\frac{\partial u}{\partial x}\right)^3, \quad \left|\frac{1}{c}\frac{\partial u}{\partial x}\right| < 1 \tag{2}$$

By deploying the Boussinesq approximation and above assumptions, the governing equations are given by:

Mass conservation:

$$\frac{\partial u}{\partial x} + \frac{\partial v}{\partial y} = 0 \tag{3}$$

Momentum equation

$$u\frac{\partial u}{\partial x} + v\frac{\partial v}{\partial y} = \left(\nu + \frac{1}{\rho c \beta *}\right)\frac{\partial^2 u}{\partial y^2} - \frac{1}{2\rho c^3 \beta *}\left(\frac{\partial u}{\partial y}\right)^2\frac{\partial^2 u}{\partial y^2} + g\beta'(T - T_\infty) \tag{4}$$

Energy (heat) equation

$$\rho c_p\left(u\frac{\partial T}{\partial x} + v\frac{\partial T}{\partial y}\right) = -\nabla.q + \tau^*\left\{\frac{D_T}{T_\infty}\left(\frac{\partial T}{\partial y}\right)^2 + D_B\frac{\partial T}{\partial y}\frac{\partial T}{\partial y}\right\} - \frac{\partial q_r}{\partial y} \tag{5}$$

Nanoparticle concentration equation

$$u\frac{\partial C}{\partial x} + v\frac{\partial C}{\partial y} = \frac{D_T}{T_\infty}\frac{\partial^2 T}{\partial y^2} + D_B\frac{\partial^2 C}{\partial y^2} \tag{6}$$

Here the following notation applies: μ is dynamic viscosity, ρ is density of the fluid, c and β* are the Eyring-Powell parameters, g is the acceleration due to gravity, τ* is the non-Fourier parameter, $\nu = \frac{\mu}{\rho}$ denotes kinematic viscosity, α stand for thermal diffusivity, c_p is heat capacity, q_r is the radiative flux, D_B and D_T represent the Brownian diffusion coefficient and thermophoretic diffusion coefficient of the species in the revised Buongiorno nanoscale model. The Buongiorno model is used to simulate nanoscale effects of the Eyring-Powell fluid conveying nano-sized particle. It is a non-homogeneous two component model (Base fluid + nanoparticles). Thus, a general nanoparticle species is considered since

this model is independent of shape and type of nanoparticle. It considers and focuses on the effect of thermophoresis and Brownian motion of nanoparticles. Further, T and C are temperature of the fluid and nanoparticle species concentration. In the Catteneo-Christov model, conductive heat flux q satisfies:

$$q + k\nabla T = -\lambda\left[\frac{\partial q}{\partial t} + V.\nabla q + (\nabla.V)q - q.\nabla V\right] \tag{7}$$

Here, k designates thermal conductivity and λ represents thermal relaxation. The Fourier model can be deduced from the Cattaneo-Christov model (7) by considering $\lambda = 0$. Now, using q from Eqns. (5) and eq. (7), the energy equation becomes:

$$u\frac{\partial T}{\partial x} + v\frac{\partial T}{\partial y} = \alpha\frac{\partial^2 T}{\partial y^2} - \lambda\left\{u\frac{\partial U}{\partial x}\frac{\partial T}{\partial x} + u\frac{\partial V}{\partial x}\frac{\partial T}{\partial y} + v\frac{\partial U}{\partial y}\frac{\partial T}{\partial x} + v\frac{\partial V}{\partial y}\frac{\partial T}{\partial y} + u^2\frac{\partial^2 T}{\partial x^2} + 2uv\frac{\partial^2 T}{\partial x\partial y} + v^2\frac{\partial^2 T}{\partial y^2}\right\}$$
$$+\tau\left\{\frac{D_T}{T_\infty}\left(\frac{\partial T}{\partial y}\right)^2 + D_B\frac{\partial C}{\partial y}\frac{\partial T}{\partial y}\right\} \tag{8}$$

The respective boundary conditions are:

$$\text{At } y = 0, \quad v = 0,\ u = U(x),\ \ -k\frac{\partial T}{\partial y} = h(T_w - T),\ D_B\frac{\partial C}{\partial y} + \frac{D_T}{T_\infty}\frac{\partial T}{\partial y} = 0 \tag{9}$$

$$\text{As } y \to \infty,\ \mathrm{u} = 0, \mathrm{T} = \mathrm{T}_\infty, \mathrm{C} = \mathrm{C}_\infty \tag{10}$$

Introducing non-similar transformations:

$$\psi = \nu\,\mathrm{Re}^{1/2}\ f(\eta,\xi),\ \ \eta = \frac{y}{x}\mathrm{Re}^{1/2},\ \ \xi = \frac{Gr_x}{\mathrm{Re}_x{}^2} \tag{11}$$

Here ψ is a dimensionless stream function, ξ, η are streamwise and transverse coordinates, $Gr_x = \frac{g\beta\Delta T x^3}{\upsilon^2}$ and $\mathrm{Re}_x = \frac{Ux}{\upsilon}$ are local (thermal) Grashof number and local Reynolds number, respectively. The parameter ξ also represents the local mixed convection. For forced convection, parameter ξ approaches zero near the leading edge and for natural convection, ξ is much larger. Here the following forms of wall stretching surface velocity, surface temperature and surface nanoparticle volume fraction are considered:

$$\mathrm{U(x)} = \mathrm{U}_0\mathrm{x}\ ,\ \mathrm{(x)} = \mathrm{T}_0\mathrm{x}^2\ ,\ \Delta\mathrm{C(x)} = \mathrm{C}_0\mathrm{x}^2 \tag{12}$$

After introducing these dimensionless variables in the governing equations (3)-(6), the emerging non-similar transformed equations take the following form:

$$(1+\varepsilon)\,f''' + ff'' - (f')^2 - \varepsilon\delta(f'')^2\ f''' + \xi\theta = -\xi\left(f''\frac{\partial f}{\partial\xi} - f'\frac{\partial f'}{\partial\xi}\right) \tag{13}$$

$$\frac{1}{\Pr}(1+R)\theta'' - 2\theta f' + f\theta' - \beta\left\{\frac{\partial\theta}{\partial\xi}\left(5\xi f'^2 + \xi^2\frac{\partial f'}{\partial\xi}f' - \xi^2 f''\frac{\partial f}{\partial\xi} - \xi f f''\right) + \theta''\left(f^2 + 2\xi\frac{\partial f}{\partial\xi}f + \xi^2\left(\frac{\partial f}{\partial\xi}\right)^2\right)\right.$$
$$\left. - \frac{\partial\theta'}{\partial\xi}\left(2\xi^2 f'\frac{\partial f}{\partial\xi} + 2\xi f f'\right) + \theta\left(4f'^2 - 2ff'' - 2\xi f''\frac{\partial f}{\partial\xi} + 2\xi\frac{\partial f'}{\partial\xi}f'\right)\right\} \tag{14}$$
$$+\theta'\left(\xi\frac{\partial f}{\partial\xi}f - 4\xi\frac{\partial f}{\partial\xi}f' - 2ff' + \xi^2\frac{\partial f'}{\partial\xi}\frac{\partial f}{\partial\xi}\right) + Nb\theta'\phi' + Nt\theta'^2 = -\xi\left(\theta'\frac{\partial f}{\partial\xi} - f'\frac{\partial\theta}{\partial\xi}\right)$$

$$\frac{1}{Sc}\phi'' - 2f'\phi + f\phi' + \frac{Nt}{Nb}\theta'' = \xi\left(\frac{\partial\phi}{\partial\xi}f' - \frac{\partial f}{\partial\xi}\phi'\right) \tag{15}$$

The transformed boundary conditions become:

$$f'(0,\xi) = 1\ ,\ \ f(0,\xi) = 0\ \ \theta'(0,\xi) = \gamma(\theta(0,\xi) - 1)\ ,\ \ Nb\phi'(0,\xi) + Nt\theta'(0,\xi) = 0 \tag{16}$$

$$f'(\eta,\xi) = 0\ ,\ \theta(\eta,\xi) = 0\ ,\ \phi(\eta,\xi) = 0 \qquad \text{as} \quad \eta\to\infty \tag{17}$$

Here primes represent derivatives with respect to η, ε and δ denote non-Newtonian rheological material fluid parameters, Pr is the Prandtl number, function f (ξ, η) is dimensionless velocity, function θ (ξ, η) is temperature, function ϕ (ξ, η) is nanoparticle species, γ is thermal Biot number (convective wall parameter), β is the thermal relaxation parameter, Nb is Brownian motion parameter, Sc is Schmidt number, Nt is thermophoresis parameter, R is radiative parameter. The dimensionless numbers are defined as follows:

$$\varepsilon = \frac{1}{\rho\beta c\upsilon}, \Pr = \frac{\upsilon}{\alpha},\ \gamma = \frac{hx}{k(\mathrm{Re})^{1/2}} \text{ and } \delta = \frac{\upsilon^2(\mathrm{Re})^3}{2c^2x^4},\ Sc = \frac{D_B}{\alpha},$$

$$Nt = \frac{\tau D_T\Delta T}{T_\infty\nu},\quad Nb = \frac{\tau D_T\Delta C}{\nu},\quad R^* = \frac{16\sigma^* T_\infty^{\ 3}}{3k^*\alpha\rho c_p},\ \beta = \frac{\tau^*}{\rho c_p} \tag{18}$$

Having determined the dimensionless variables (f, θ *and* ϕ), by numerical solution of the two-parameter nonlinear problem derived by Eqns. (13)-(17), which is elaborated in due course, we can then evaluate engineering design quantities. These are local skin friction coefficient c_f (lead to find wall shear stress), local Nusselt number Nu (helps to find heat transfer rate) and Sherwood number Sh (nanoparticle species (mass) transfer rate) which are defined respectively with the following expressions:

$$c_f = \mu\frac{2\tau_w(x)}{\rho(U(x))^2},\qquad Nu = \frac{q_w(x)x}{k\Delta T} \qquad \text{and } Sh = \frac{m_w(x)x}{k\Delta C} \tag{19}$$

Here the following definitions apply:

$$\tau_{\mathrm{w}} = \left[\mu\frac{\partial \mathrm{u}}{\partial \mathrm{y}} - \frac{1}{6\beta * \mathrm{c}^3}\left(\frac{\partial \mathrm{u}}{\partial y}\right)^3 + \frac{1}{\beta * \mathrm{c}}\frac{\partial \mathrm{u}}{\partial \mathrm{y}}\right]_{\mathrm{y}=0}, q_w = -k\left(\frac{\partial T}{\partial y}\right)_{y=0}, \; m_w = -k\left(\frac{\partial C}{\partial y}\right)_{y=0} \tag{20}$$

Furthermore, introducing the transformations from Eqn. (18), dimensionless skin friction, Nusselt number and Sherwood number take the form:

$$\mathrm{Re}^{1/2}\, c_f = 2(\varepsilon+1) f''(0,\xi) - \frac{2\varepsilon\left(f''(0,\xi)\right)^3 \delta}{3} \tag{21}$$

$$\mathrm{Re}^{-1/2}\,\mathrm{N\,u} = -\theta'(0,\xi) \tag{22}$$

$$\mathrm{Re}^{-1/2}\,\mathrm{S\,h} = -\phi'(0,\xi) \tag{23}$$

3. NUMERICAL SOLUTIONS

3.1- SPARROW-YU LOCAL NON-SIMILARITY METHOD (LNM) SOLUTION

Flow problems do not necessarily possess similarity solutions. Frequently complex thermophysical phenomena such as mixed convection from vertical surfaces with convective boundary conditions generate generally non-similar parabolic boundary value problems. To deal with such non-similar problems, Sparrow and Yu [47] introduced the robust local non-similarity method which is also further explained in Minkowycz et al. [48]. In this method, the terms containing $\xi-$derivatives are first neglected to obtain a local similarity solution; next to obtain local non-similarity solutions, the $\xi-$ derivatives are considered as another dependent function. Massoudi [49] used local non-similarity method to compute non-Newtonian fluid flow over the surface of wedge. Bég et al. [50] investigated inclined solar collector thin film boundary layer flows with local non-similarity method. Bég et al. [51] computed the hydromagnetic convection from a stretching plate in porous media using local non-similarity method. Mushtaq et al. [52] implemented local non-similarity method with second level of truncation to study mixed convection flow with effect of radiation, benchmarking solutions with a Shanks series-extended perturbation method and non-similarity method. Roy and Hossain [53] computed the convective flow from vertical plate with variable surface temperature using local non-similarity method. Chamkha et al. [54] examined the nanofluid flow over a sphere suspended in a porous medium using local non-similarity method.

Local Similarity method:

Local similarity method admits solutions and transforms the governing equation into system of coupled and nonlinear ordinary differential equation provided the non-similarity term is very small and may be negated. To apply local similarity method to Eqns. (13)-(17), the terms on right hand side which contain $\xi.\frac{\partial(.)}{\partial\xi}$ are removed under the assumption that these $\xi-$ derivatives terms are very small which is valid for $\xi<<1$. Hence, the system of equations becomes:

$$(1+\varepsilon)\, f'''-(f')^2+ff''-\varepsilon\delta(f'')^2\, f'''+\xi\theta=0 \tag{24}$$

$$\frac{1}{\Pr}(1+R)\theta''-2\theta f'+\theta' f-\beta\left[4f'^2\theta+\theta'' f^2-3ff'\theta'-2ff''\theta\right]+Nb\theta'\phi'+Nt\theta'^2=0 \tag{25}$$

$$\frac{1}{Sc}\phi''+f\phi'-2f'\phi+\frac{Nt}{Nb}\theta''=0 \tag{26}$$

The associated boundary conditions:

$$f'(0,\xi)=1\ ,\ \ f(0,\xi)=0\ \theta'(0,\xi)=\gamma(\theta(0,\xi)-1)\ ,\ \ Nb\phi'(0,\xi)+Nt\theta'(0,\xi)=0 \tag{27}$$

$$f'(\eta,\xi)=0\ ,\ \theta(\eta,\xi)=0\ ,\ \phi(\eta,\xi)=0 \qquad \text{as}\ \ \eta\to\infty \tag{28}$$

Eqns. (24)-(28) can be viewed as a coupled non-linear ordinary differential boundary value problem by taking ξ as a parameter for a given Pr, Sc, Nt, Nb and ε.

Local Non-Similarity Method:

The solutions gained by neglecting the terms containing ξ-derivative of f, θ and ϕ are of undesirable precision. To improve the accuracy, these derivatives must be considered in the equations. The local non-similarity method (LNM) includes the streamwise derivative by considering these derivatives as another dependent function and auxiliary equations for these new functions. We consider the terms $\frac{\partial f}{\partial\xi}$, $\frac{\partial\theta}{\partial\xi}$ and $\frac{\partial\phi}{\partial\xi}$ as dependent functions, so introducing the following functions:

$$P(\eta,\xi)=\frac{\partial f}{\partial\xi},\quad Q(\eta,\xi)=\frac{\partial\theta}{\partial\xi},\quad R(\eta,\xi)=\frac{\partial\phi}{\partial\xi} \tag{29}$$

The governing Eqns. (13)-(17) are as follows:

$$(1+\varepsilon) f''' - (f')^2 + ff'' - \delta\varepsilon (f'')^2 f''' + \xi\theta = \xi (P'f' - Pf'') \tag{30}$$

$$\begin{aligned}\frac{1}{\Pr}\theta'' - 2\theta f' + f\theta' - \beta\Big[& Q\left(5\xi f'^2 + \xi^2 P'f' - \xi ff'' - \xi^2 Pf''\right) + \theta''\left(\xi^2 (P)^2 + f^2 + 2\xi fP\right) \\ & - Q'\left(2\xi ff' + 2\xi^2 fP\right) + \theta'\left(\xi fP - 2ff' + \xi^2 PP' - 4\xi fP\right) \\ & + \theta\left(4f'^2 - 2ff'' + 2\xi P'f' - 2\xi Pf''\right)\Big] + Nb\theta'\phi' + Nt\theta'^2 = \xi\left(fQ - \theta' P\right)\end{aligned} \tag{31}$$

$$\frac{1}{Sc}\phi'' + f\phi' - 2f'\phi + \frac{Nt}{Nb}\theta'' = \xi\left(fR - \phi' P\right) \tag{32}$$

$$f'(0,\xi) = 1,\ f(0,\xi) = 0,\ \theta'(0,\xi) = \gamma(\theta(0,\xi) - 1),\ \ Nt\theta'(0,\xi) + Nb\phi'(0,\xi) = 0 \tag{33}$$

$$f'(\infty,\xi) = 0,\ \theta(\infty,\xi) = 0,\ \phi(\infty,\xi) = 0 \tag{34}$$

Additional equations for functions, P, Q, R and the associated conditions at the boundaries can be formed by considering the derivatives of equations (30) - (34) with respect to ξ:

$$(1+\varepsilon) g''' + fP' + 2f''P - 3f'P' - \varepsilon\delta(P'''f''^2 + 2f'''f''P'') + \theta + \xi\phi = \xi\left(P^2 - PP''\right) \tag{35}$$

$$\begin{aligned}\frac{1}{\Pr}(1+R^*)Q'' + 2P\theta' + fQ' - 3Qf' - 2\theta P' + NbQ'\phi' + Nb\theta' R' + 2Nt\theta' Q' - \xi\left(P'Q - Q'P\right) \\ - \beta\Big[Q''\left(f^2 + \xi^2 (P)^2 + 2\xi fP\right) - Q'\left(4ff' - \xi fP + 10\xi f'P + 2\xi f'P + \xi^2 PP'\right) \\ + Q\left(9f'^2 + 14\xi f'P' + \xi^2 P'^2 - 3ff'' - 5\xi Pf'' - \xi fP'' - \xi^2 PP''\right) + \theta''\left(4fP + 4\xi P^2\right) \\ + \theta'\left(fP + \xi P^2 - 6f'P - 2fP' - 2\xi PP'\right) + \theta\left(10f'P' - 4Pf'' + 2\xi P'^2 - 2fP'' - 2\xi PP''\right)\Big] = 0\end{aligned} \tag{36}$$

$$\frac{1}{Sc}R'' + R'f + 2\phi' P - 3f'R - 2\phi P' + \frac{Nt}{Nb}Q'' - \xi\left(RP' - PR'\right) \tag{37}$$

$$P'(0,\xi) = 0\ ,\ P(0,\xi) = 0, Q'(0,\xi) = \gamma Q(0,\xi),\ NbR'(0,\xi) + NtQ'(0,\xi) = 0 \tag{38}$$

$$P'(\infty,\xi) = 0,\ Q(\infty,\xi) = 0,\ R(\infty,\xi) = 0 \tag{39}$$

The terms $\frac{\partial P}{\partial \xi}$, $\frac{\partial Q}{\partial \xi}$, $\frac{\partial R}{\partial \xi}$ and their higher order derivatives with regard to ξ are assumed to be very small and hence are omitted. The system of coupled equations is now considered to give more accurate results as compared to the local similarity system of equations in which streamwise derivative are neglected. The local non-similarity method comparison with HAM is given in **Table 1** and found outstanding accordance is obtained. Confidence in both methods is therefore justifiably high.

3.2 SOLUTION BY HAM

To further validate the LNM Solutions, an alternative technique has been deployed to solve the transformed equations defined by Eqns. (13)-(17). The homotopy analysis method (HAM), a significantly accurate and robust method initiated by Liao [54], is selected here to solve the nonlinear

system of equations. HAM is a widely used method which overcomes the restrictions of traditional perturbation methods. HAM has been widely implemented to solve many boundary value problems in modern nonlinear fluid dynamics and nanofluid mechanics including Casson magnetic bio-convectional nanofluid flow over unsteady stretching surface [56], peristaltic biomechanical pumping [57], non-Newtonian oscillatory flow [58], electrically-conducting mixed convection nanofluid flow from vertical cylinder under static radial magnetic field [59], reactive viscoelastic magneto-convection from an exponential stretching surface [60], transient nanofluid flow from a rotating sphere, hydromagnetic micropolar convection in a thermal duct with entropy generation [62], thermal polymeric micropolar Falkner-Skan coating flows with viscous heating [63] and most recently unsteady hydromagnetic pumping of ionized gas in revolving MHD generator [64]. HAM has consistently demonstrated excellent flexibility, accuracy and convergence in all these areas. The HAM solution for the non-similar Eqns. (13) - (15) with boundary conditions (16) and (17) can be obtained using HAM by selecting favourable initial approximations, auxiliary parameters (h_1 , h_2 and h_3), linear operators ($\mathrm{L}_1(f)$, $\mathrm{L}_2(\theta)$ and $\mathrm{L}_3(\phi)$), non-linear operators ($\mathrm{N}_1(f,\theta,\phi), \mathrm{N}_2(f,\theta,\phi)$ and $\mathrm{N}_3(f,\theta,\phi)$) and zeroth order deformation equations. The chosen initial guesses are:

$$f_0 = 1 - e^{-\eta} \tag{40 a}$$

$$\theta_0 = \frac{\gamma}{\gamma+1} e^{-\eta} \tag{40 b}$$

$$\phi_0 = -\frac{Nt}{Nb}\frac{\gamma}{\gamma+1} e^{-\eta} \tag{40 c}$$

The linear operators are taken as

$$\mathrm{L}_1(f) = f''' - f' \tag{41 a}$$

$$\mathrm{L}_2(\theta) = \theta'' - \theta \tag{41 b}$$

$$\mathrm{L}_3(\phi) = \phi'' - \phi \tag{41 c}$$

satisfying properties

$$\mathrm{L}_1(A_1 + A_2 e^{\eta} + A_3 e^{-\eta}) = 0 \tag{42 a}$$

$$\mathrm{L}_2(A_4 e^{\eta} + A_5 e^{-\eta}) = 0 \tag{42 b}$$

$$\mathrm{L}_3(A_6 e^{\eta} + A_7 e^{-\eta}) = 0 \tag{42 c}$$

Here, A_i's $(1 \le i \le 7)$ are constants. Suppose $0 \le p \le 1$ is Liao embedding parameter. h_1, h_2 *and* h_3 are control parameters., then zeroth-order deformation equations can be formed as:

$$(1-p)\mathrm{L}_1[f(\eta,\xi;p) - f_0(\eta,\xi)] = p h_1 \mathrm{N}_1 \tag{43 a}$$

$$(1-p)\mathrm{L}_2[\theta(\eta,\xi;p)-\theta_0(\eta,\xi)]=ph_2\mathrm{N}_2 \quad (43\text{ b})$$

$$(1-p)\mathrm{L}_3[\phi(\eta,\xi;p)-\phi_0(\eta,\xi)]=ph_3\mathrm{N}_3 \quad (43\text{ c})$$

Where $\mathrm{N}_1(f,\theta,\phi)$, $\mathrm{N}_2(f,\theta,\phi)$ and $\mathrm{N}_3(f,\theta,\phi)$ are the nonlinear operators formed from non-linear Eqns. (13)-(15). The associated conditions:

$$f'(\eta,\xi;p)\big|_{\eta\to 0}=1,\ f(\eta,\xi;p)\big|_{\eta\to 0}=0 \text{ and } f'(\eta,\xi;p)\big|_{\eta\to\infty}=0 \quad (44\text{ a})$$

$$\theta'(\eta,\xi;p)\big|_{\eta\to 0}=\gamma(\theta(0,\xi;p)\big|_{\eta\to 0}-1)\ ,\ \theta(\eta,\xi;p)\big|_{\eta\to\infty}=0 \quad (44\text{ b})$$

$$Nb\phi'(\eta,\xi;p)\big|_{\eta\to 0}+Nt\theta'(\eta,\xi;p)\big|_{\eta\to 0}=0,\ \phi(\infty,\xi;p)=0 \quad (44\text{ c})$$

Now constructing the mth order deformation equations by considering auxiliary functions $\mathrm{H}_1(\eta,\xi)=\mathrm{H}_2(\eta,\xi)=\mathrm{H}_3(\eta,\xi)=1$

$$\mathrm{L}_1[f_m(\eta,\xi)-\chi_{m-1}f_{m-1}(\eta,\xi)]=h_1\mathrm{H}_1R_m{}^f(\eta,\xi) \quad (45\text{ a})$$

$$\mathrm{L}_2[\theta_m(\eta,\xi)-\theta_{m-1}(\eta,\xi)]=h_2\mathrm{H}_2R_m{}^\theta(\eta,\xi) \quad (45\text{ b})$$

$$\mathrm{L}_3[\phi_m(\eta,\xi)-\chi_{m-1}\phi_{m-1}(\eta,\xi)]=h_3\mathrm{H}_3R_m{}^\phi(\eta,\xi) \quad (45\text{ c})$$

Where $\chi_m=1$ if $m>1$ and $\chi_m=0$ if $m\le 1$. Also, $R_m{}^f(\eta,\xi)$, $R_m{}^\theta(\eta,\xi)$ and $R_m{}^\phi(\eta,\xi)$ are residual functions. Validation of present results with the earlier solutions of Mushtaq et al. [52] for both HAM and LNM are documented in **Table 1**.

Table 1. Comparing current output with Mushtaq et al. [52] of 50th order of approximations of $-\theta'(0,0)$ for $\gamma=1,\mathrm{Pr}=0.7,\varepsilon=1,\delta=0.2,\xi=0,\ h_1=h_2=-1.$

	$-\theta'(0,0)$		
Pr	Mushtaq et al. [52]	HAM Results	LNM Results
1	1.3349	1.33333	1.33345
5	3.2927	3.31651	3.31669
10	4.7742	4.78967	4.78976

3.2-1 CONVERGENCE OF HAM

The m[th] order deformation equations corresponding to Eq. (13) - (17) is formulated using the above initial approximation f_0, θ_0 and ϕ_0, linear $\mathcal{L}_1(\mathrm{f})$, $\mathcal{L}_2(\theta)$ and $\mathcal{L}_3(\theta)$ operators, nonlinear operators $\mathcal{N}_1$, $\mathcal{N}_2$ and $\mathcal{N}_3$ and appropriate values for the auxiliary parameters h_1, h_2 *and* h_3 are $-0.2<\mathrm{h}_1<0.8$, $-0.2<h_2<1.25$ and $-0.2<h_3<1.25$. This range of auxiliary parameters is obtained using symbolic software **MATHEMATICA** and the variation between $f''(0,\xi)$, $\theta'(0,\xi)$ and $\phi'(0,\xi)$ vs. $\hbar=h_1,h_2,h_3$ is shown in **Fig. 2**. Finally, solutions (49 a) – (49 c) are obtained. **Fig. 3** explores how residual error is varying with the order of approximation. It can be seen that the residual error is reduced

to less than 10^{-9} at the 20th order of the approximation. Thus, increasing approximation improves the accuracy of the series solution. The following set of parameters are used for the present computations:

$$\gamma = 0.8, \mathrm{Nt} = \mathrm{Nb} = 0.1, \mathrm{Sc} = 1,\ \delta^* = 2, \varepsilon = 0.1, \mathrm{Pr} = 1, \mathrm{R} = 0.5\ \xi = 0.5, \beta = 0.1,$$

$$h_1 = h_2 = h_3 = -0.7$$

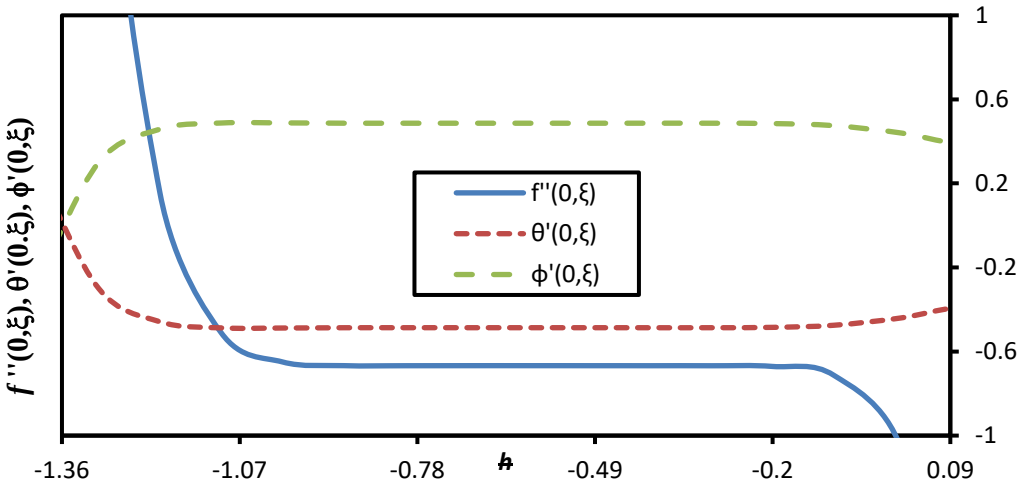

Fig.2. h-curve

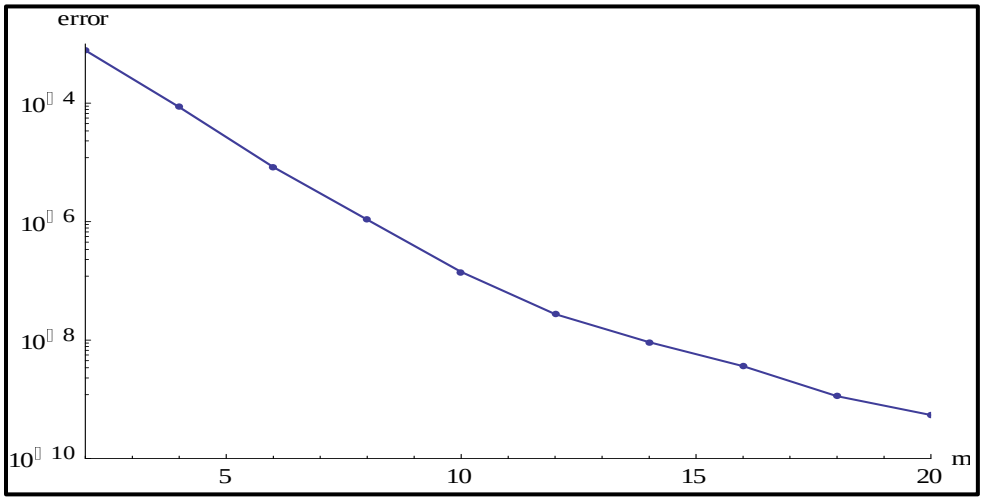

Fig 3. Residual error vs order of approximation (m)

Table 2 shows the convergence of homotopy series solutions. The convergence test has been conducted up to the 20th order of approximation ($\mathrm{m} = 20$) and sufficient convergence is attained after the 12th order of approximation. Thus, $m = 12$ is considered throughout the computation process of this study, in all subsequent figures.

Table 2. Convergence of HAM for various orders of approximation for $\varepsilon = 0.1, \delta^* = 1, \xi = 0.5, \mathrm{Pr} = 1, \beta = 0.1, \gamma = 0.8, \mathrm{Nt} = \mathrm{Nb} = 0.1, \mathrm{Sc} = 1$ $h_1 = h_2 = h_3 - 0.7$

m (order)	$-f''(0,0)$	$-\theta'(0,0)$	$\phi'(0,0)$
2	0.6605	0.48652	0.486517
5	0.66762	0.48663	0.486628
8	0.66737	0.48658	0.486576
10	0.66725	0.48656	0.48656
12	0.66726	0.48656	0.48656
15	0.66726	0.48656	0.48656
20	0.66726	0.48656	0.48656

4. HAM GRAPHICAL RESULTS AND ANALYSIS

HAM computations are visualized in Figs 3-12 for the influence of rheological parameters (Eyring-Powell parameters), thermophysical parameters (Prandtl number, radiation, thermal relaxation parameter) and Buongiorno modified nanoscale parameters on velocity, nanoparticle volume fraction and temperature. Further solutions for the local skin friction, $-f''(\xi, 0)$, Nusselt number, $\theta'(\xi, 0)$ and nanoparticle species Sherwood number, $\phi'(\xi, 0)$ are also tabulated for all parameters.

Fig. 3(a)- Fig. 3(c) elaborate the impact of mixed convection parameter on the velocity (Fig. 3(a)), temperature (Fig. 3(b)) and nanoparticle concentration (Fig. 3(c)). The thermal buoyancy force is clearly accentuated with increment in ξ (local Grashof number $\mathrm{Gr_x} = \frac{\mathrm{g\beta\Delta Tx^3}}{\upsilon^2}$ and $\xi = \frac{Gr_x}{\mathrm{Re}_x^{\,2}}$). This mobilizes more intense free convection currents which accelerates the boundary layer flow. The enhancement in momentum diffusion rate exceeds the thermal and nanoparticle species diffusion rates; exacerbating the molecular motion of the fluid particles leads to less interaction and less collision between nanoparticles and fluid particles and thus the temperature and nanoparticle concentration decreases. Momentum boundary layer thickness is therefore decreased whereas nanoparticle species and thermal boundary layer thicknesses are raised. The coating dynamics is therefore significantly impacted by stronger thermal buoyancy effect. Thus, it can be analysed that the velocity increases while temperature and nanoparticle volume fraction suppressed as ξ rises. Also Fig. 3(a)-Fig. 3(c) shows the relative response of non-Newtonian Powell-Eyring fluid conveying nano-sized particles and Newtonian fluid conveying nano-sized particle. Velocity of pseudoplastic Powell-Eyring fluid clearly exceeds that of the Newtonian fluid which confirms that shear thinning behavior of Powell-Eyring fluid encourages flow acceleration in the regime of boundary layer. Further, the nanoparticle concentration and temperature for Powell-Eyring fluid conveying nano-sized particle is smaller as compared to Newtonian

fluid conveying nano-sized particle, indicating that pseudoplasticity is an effective control mechanism for heat regulation and nanoparticle diffusion in the coating. Of course, the dynamics is confined to laminar flow which is desirable in coating processes since enhanced regulation of the deposition on the substrate is possible only with laminar growth of the boundary layer from the leading edge. The implication is that with more realistic rheological models, a more precise prediction of characteristic of heat, momentum and nanoparticle diffusion is achieved. The conventional Newtonian model deployed in many previous studies e. g. Benkreira et al. [65], Coyle [66], Pearson [67], Thompson [68] and Gaskell et al. [69] is clearly unrealistic for real polymer flows. These studies ignore the modification in flow behaviour due to actual rheological properties of industrial polymers. The present computations, in consistency with other recent studies e. g. Kumaran et al. [45] indicate that Newtonian fluids under-predict flow velocities which in turn leads to incorrect estimation in associated transport characteristics (thermal and nanoparticles).

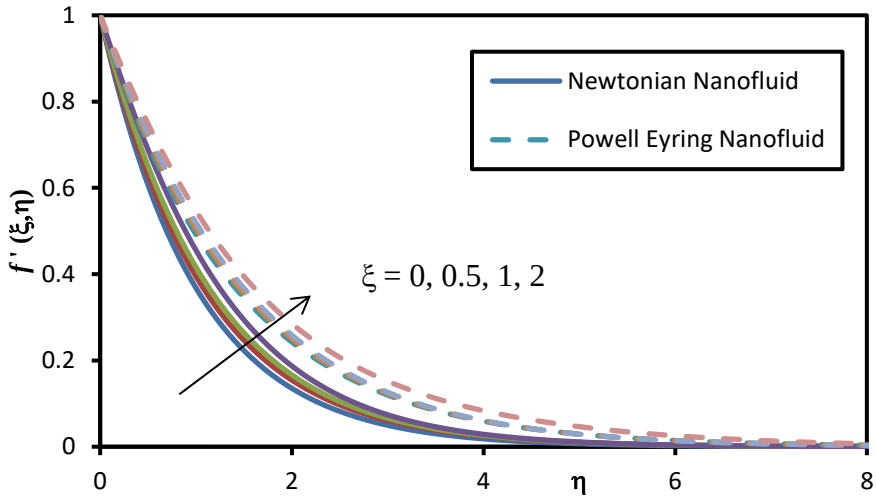

Fig.3 (a) Impact of ξ on velocity for Newtonian and Powell-Eyring Fluid

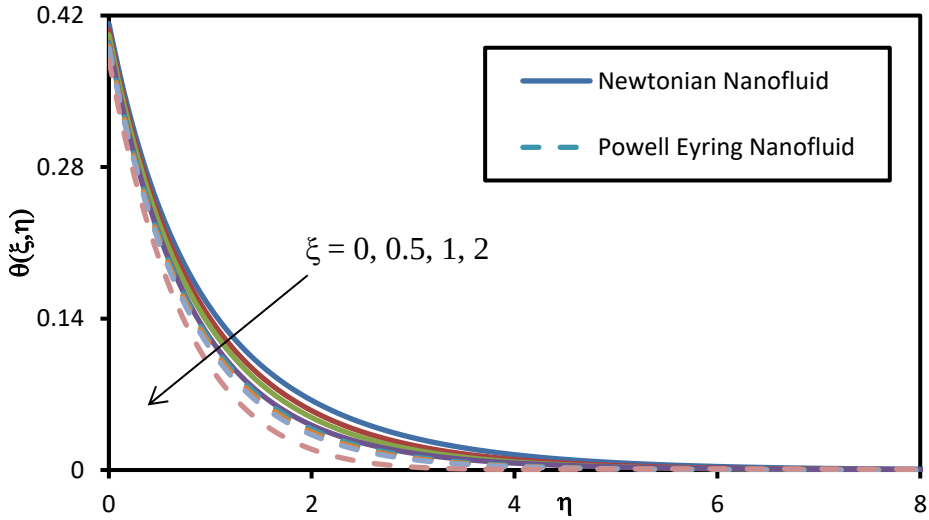

Fig.3 (b) Influence of ξ on temperature for Newtonian and Powell-Eyring Fluid

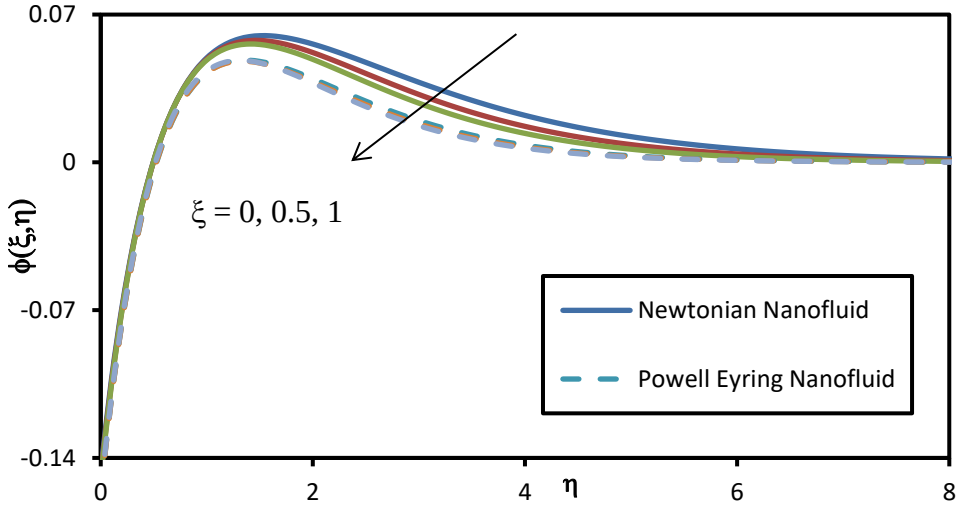

Fig.3 (c) Effect of ξ on nanoparticle concentration for Powell-Eyring and Newtonian fluid

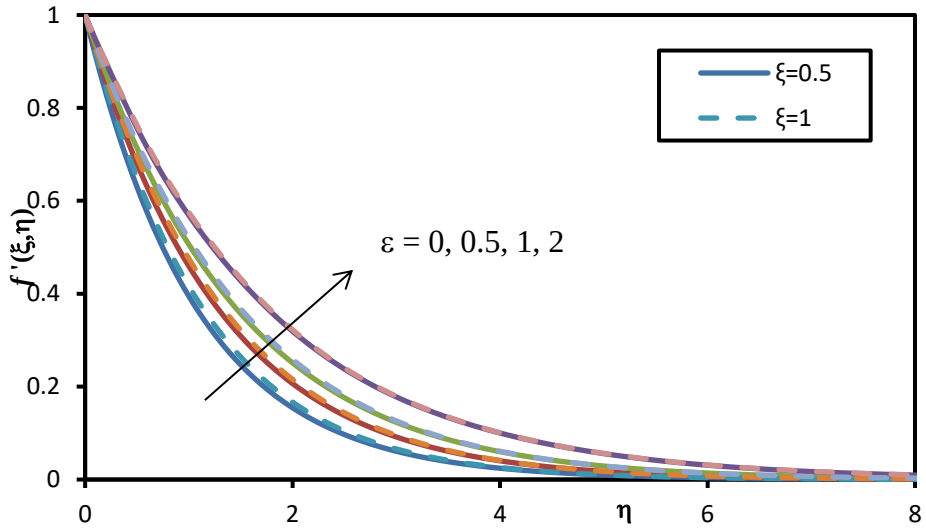

Fig.4 (a) Impact of ε on velocity

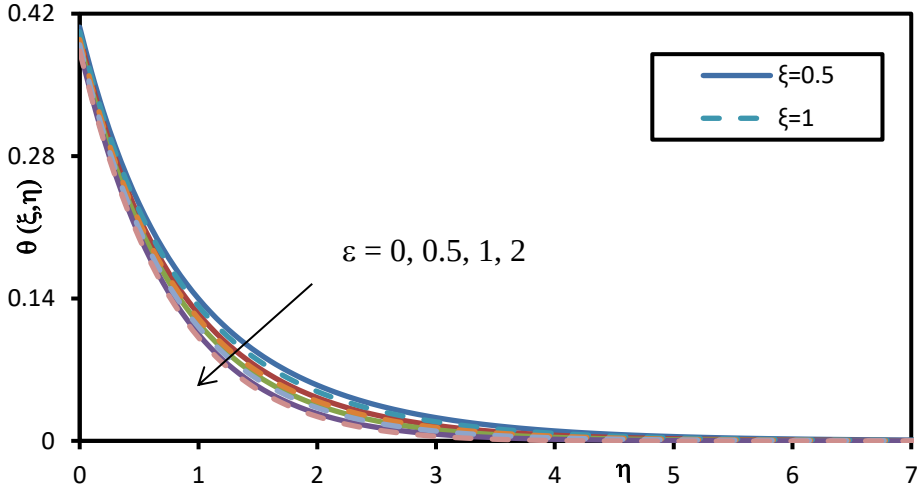

Fig.4 (b) Effect of ε on temperature regime

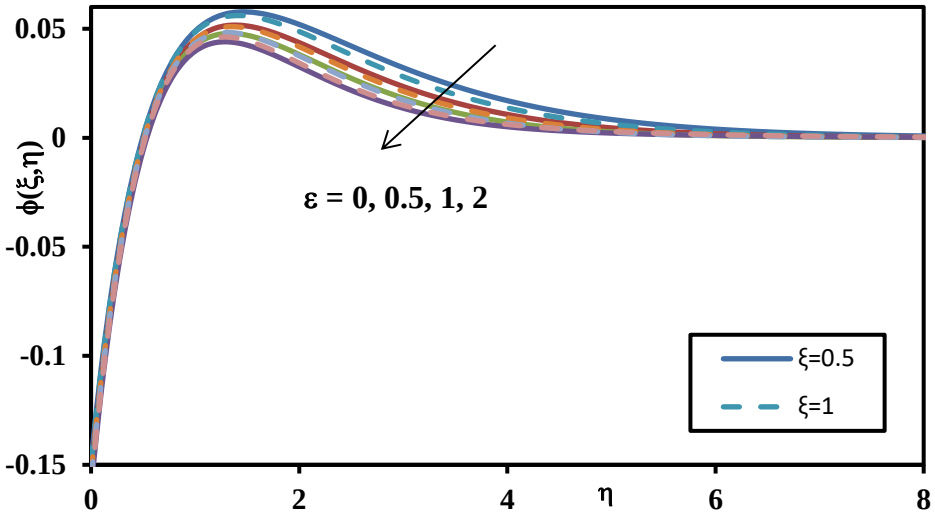

Fig.4 (c) ε influencing nanoparticle concentration

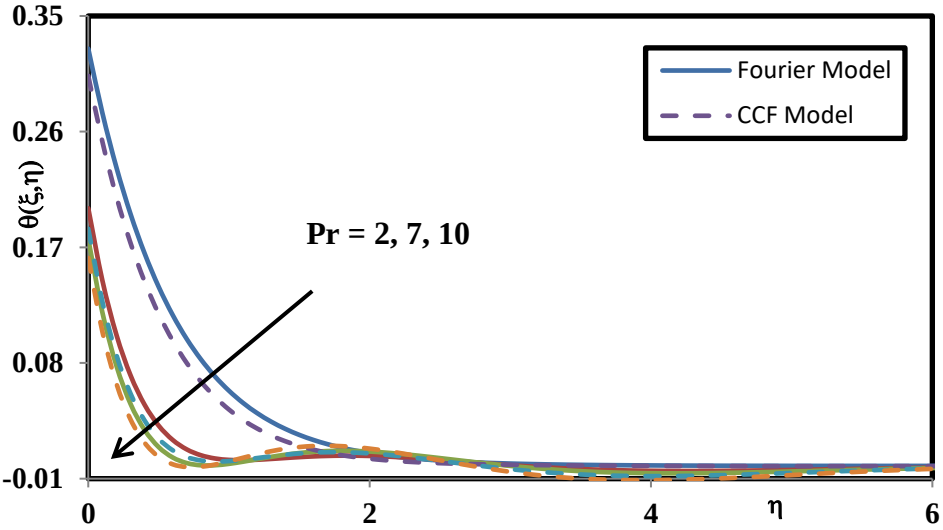

Fig.5 (a) Prandtl number (Pr) influencing temperature for Cattaneo-Christov flux (CCF) and Fourier's model

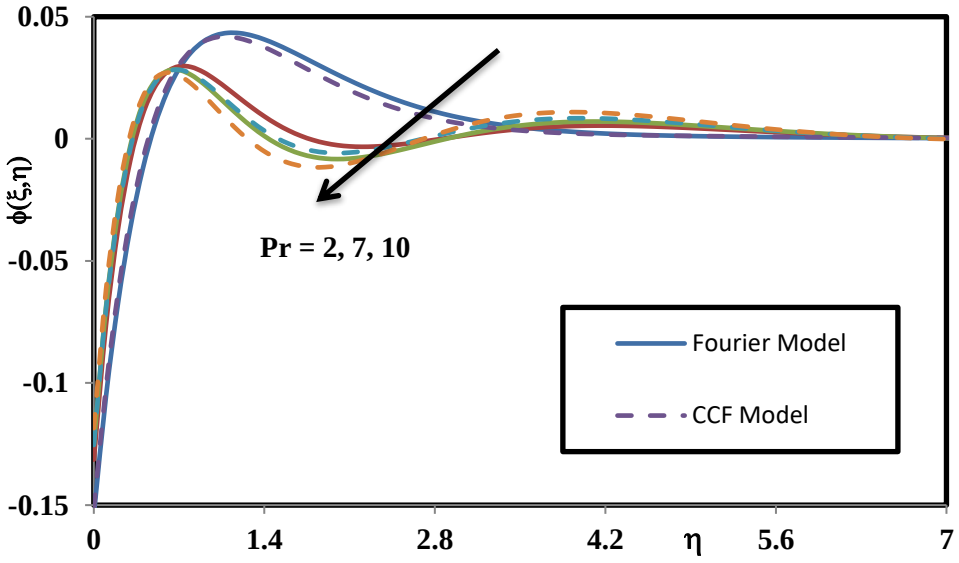

Fig.5 (b) Influence of Pr on nanoparticle volume fraction for CCF model and Fourier's model

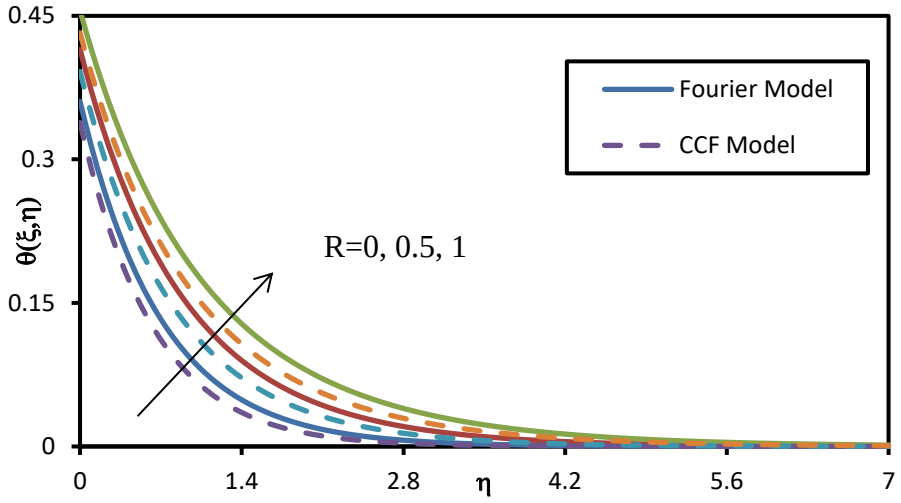

Fig.6 (a) Radiation R effecting temperature profile for Fourier's and CCF model

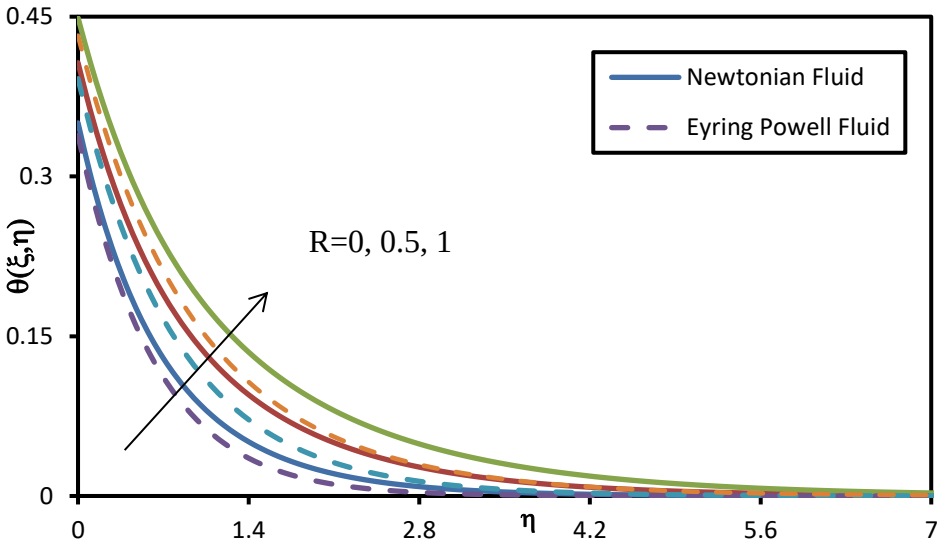

Fig.6 (b) Effect of radiation R on temperature profile for Powell-Eyring and Newtonian fluid

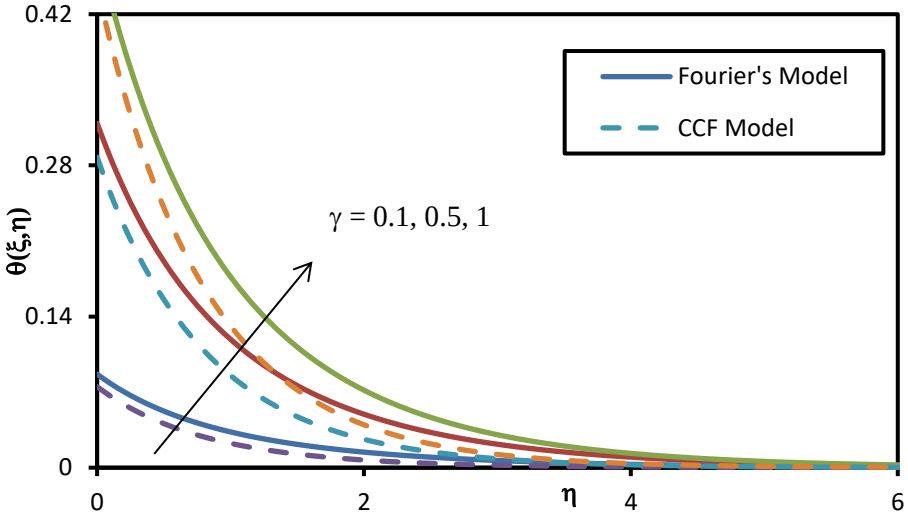

Fig.7 (a) Influence of thermal Biot number (γ) on temperature for Cattaneo-Christov model and Fourier's model

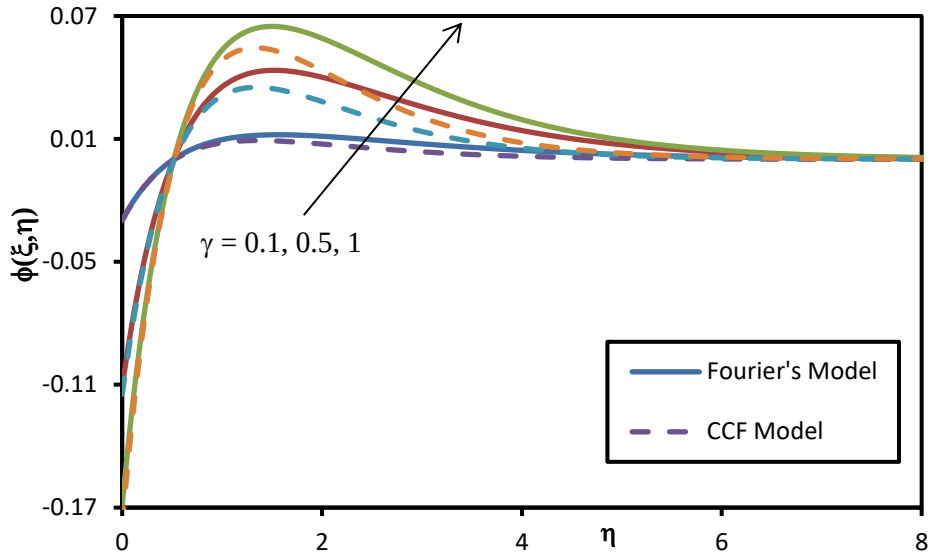

Fig.7 (b) Impact of γ on temperature for CCF model and Fourier's model

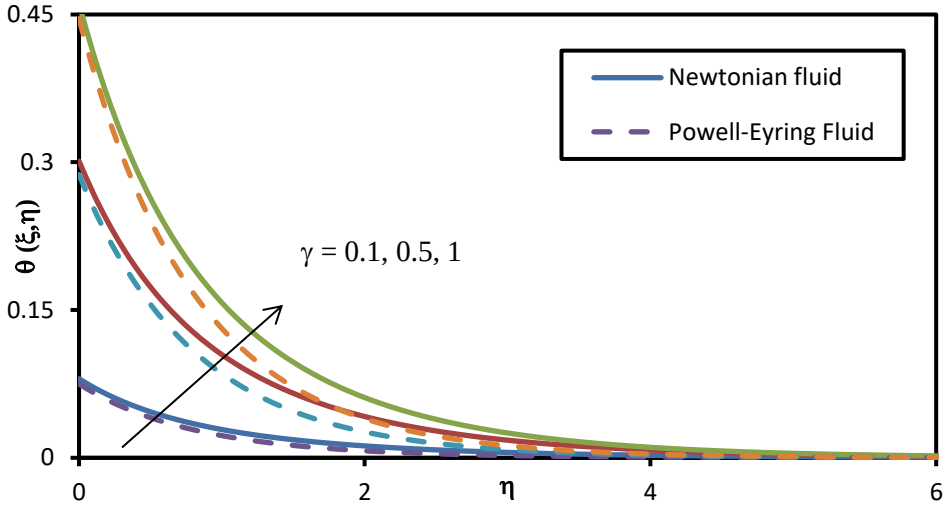

Fig.8 (a) Effect of γ on temperature for Powell-Eyring and Newtonian fluid

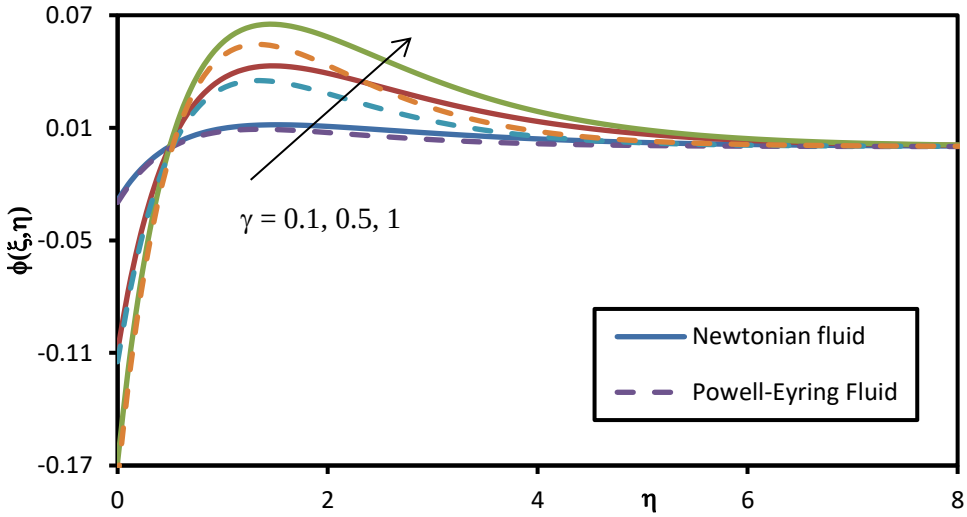

Fig.8 (b) Impact of γ on nanoparticle concentration profile for Powell-Eyring fluid and Newtonian fluid

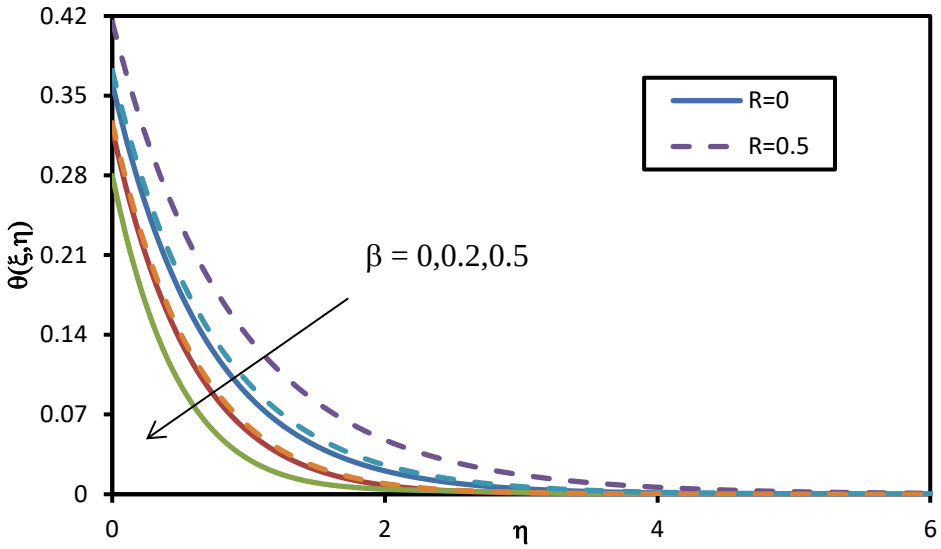

Fig.9 (a) Influence of thermal relaxation β on temperature field for radiation R

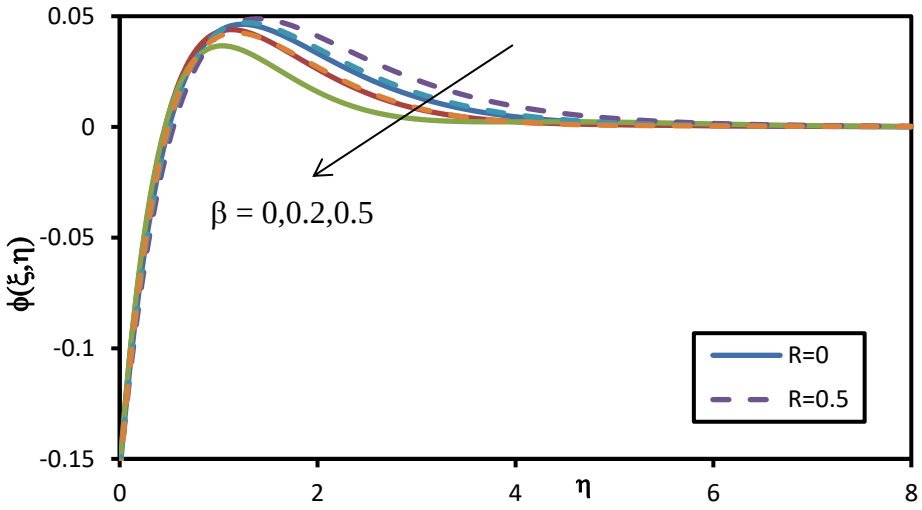

Fig.9 (b) Influence of βon nanoparticle volume fraction for radiation R

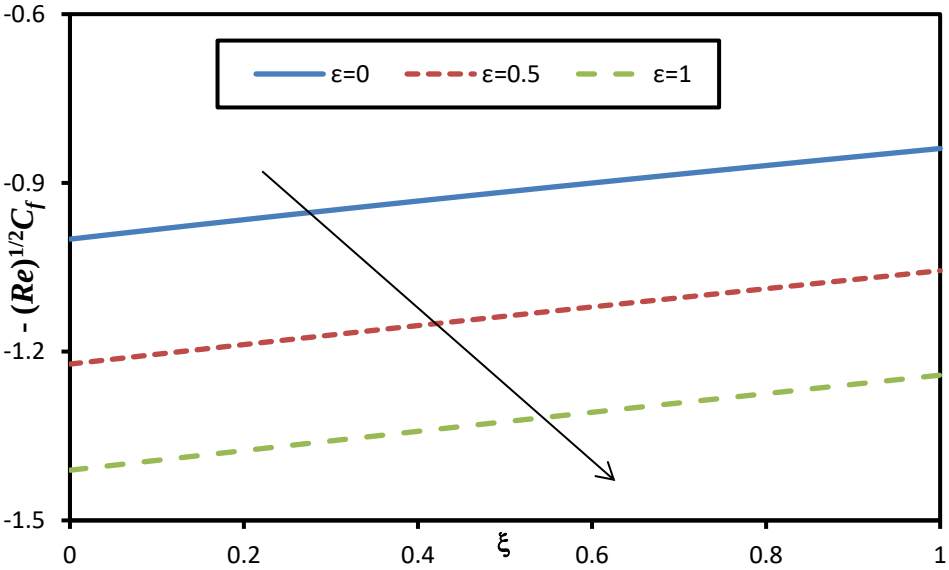

Fig.10 Impact of ε on skin friction coefficient against mixed convection parameter

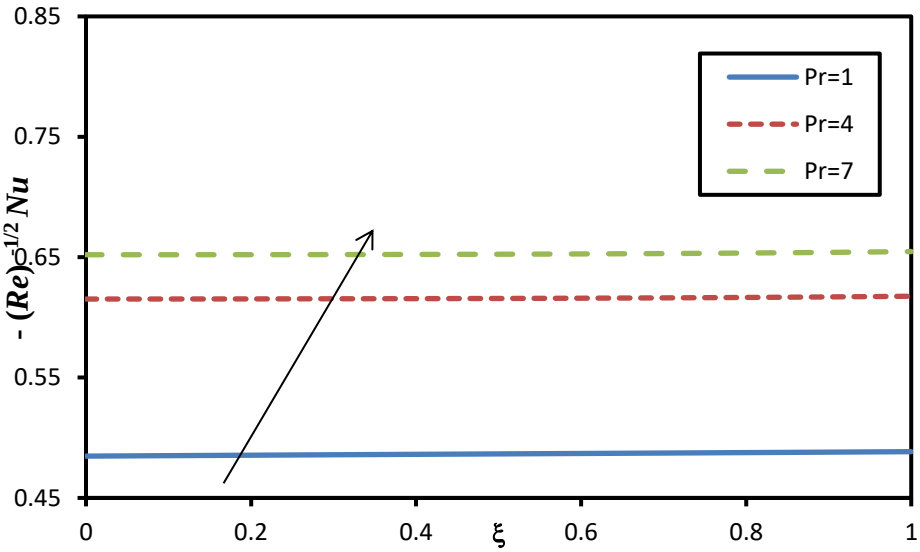

Fig.11 Impact of Pr on $\mathrm{Re}^{-1/2}$ N u against ξ

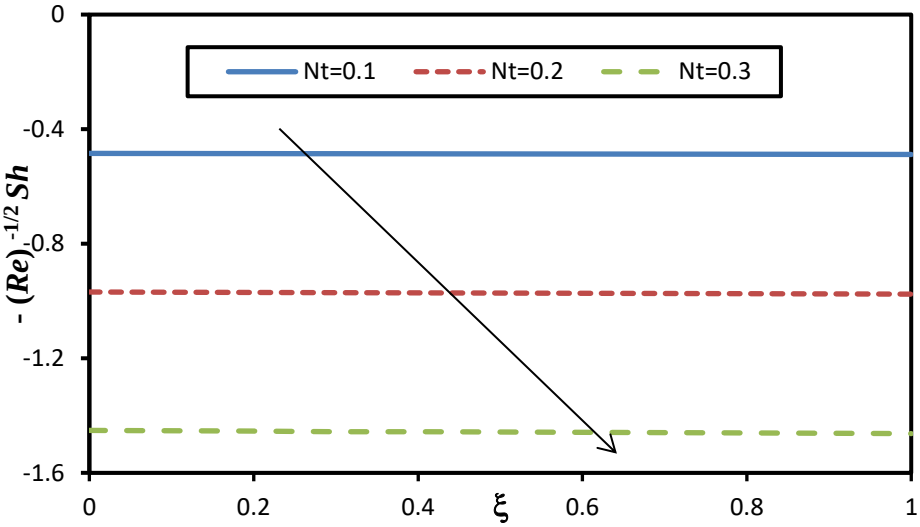

Fig.12 (a) Impact of Nt on $\mathrm{Re}^{-1/2}$ Sh against ξ

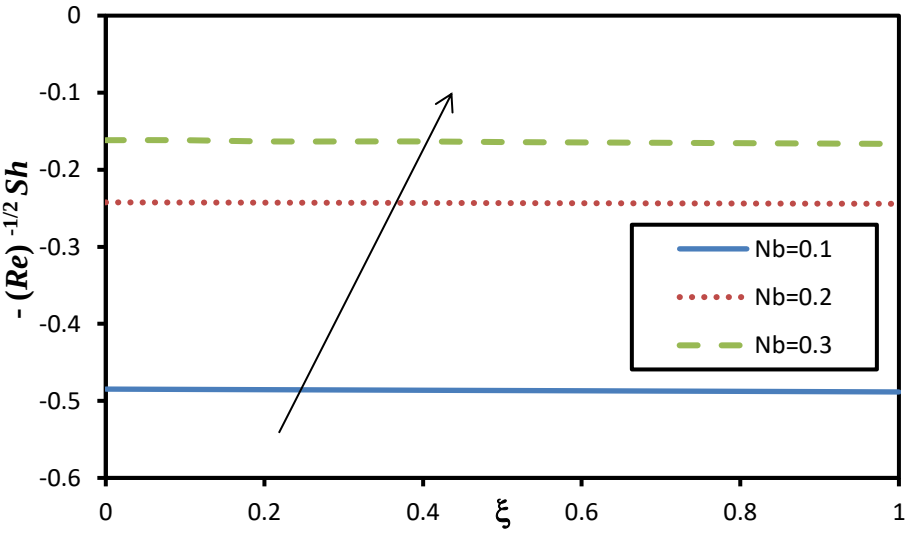

Fig.12 (b) Impact of Nb on local $\mathrm{Re}^{-1/2}$ Sh against ξ

Fig. 4(a) – Fig. 4(c) describes the impact of Eyring-Powell rheological parameter (ε) on velocity, nanoparticle fraction and temperature for various values of mixed convection parameter(ξ). For both forced (ξ =0) and progressively stronger natural convection (increment in ξ), velocity of the fluid increases while temperature and nanoparticle volume concentration decrease. $\varepsilon = 0$ corresponds to Newtonian fluid conveying nano-sized particle which clearly under-predicts velocity magnitudes. Stronger pseudoplastic rheology of the fluid conveying nano-sized particle clearly reduces momentum boundary layer thickness. Greater values of $\varepsilon = \frac{1}{\rho\beta c\upsilon}$ imply a depletion in coating fluid viscosity which reduces the viscous resistance resulting in flow acceleration. The momentum boundary layer thickness for Eyring-Powell fluid is consistently lower than Newtonian fluid. On contrary, the nanoparticle concentration and thermal boundary layer thicknesses are suppressed with elevation in Eyring-Powell fluid parameter. Fig. 4(a) –Fig. 4(c) and Fig. 3(a) - Fig. 3(c) also shows the ascendancy of mixed convection parameter and a similar response is observed.

Fig. 5(a) and Fig. 5(b) illustrate the influence of Prandtl number $(\mathrm{Pr} = 2, 7, 10)$ on temperature and nanoparticle volume fraction for both the Cattaneo-Christov flux (CCF) model and Fourier's model for heat flux. A rise in Prandtl number suppresses the temperature and nanoparticle concentration since greater Prandtl number is correlated with smaller thermal diffusivity. Temperature of fluid conveying nano-sized particle coating decreases. Higher Prandtl numbers are characteristic of polymeric coatings which feature insulation properties. It is also evident that Fourier's model (parabolic) computes higher temperatures as compared with the Cattaneo-Christov model (hyperbolic). Therefore, conventional thermal polymer coating models ignoring the finite thermal wave speed in real materials over-predict the temperatures. Thermal relaxation parameter can be considered in order to control the heat transfer in the coating along the vertical plate. Thus, the cooling and heating of coating boundary layer can be performed by increasing and decreasing Pr respectively. Similarly, this parameter can also be helpful in reducing the distribution of nanoparticle on the surface of the plate.

Fig. 6(a) and Fig. 6(b) explain the impact of thermal radiation R on temperature and nanoparticle volume fraction profiles corresponding to Fourier and non-Fourier Cattaneo-Christov model, respectively. $\mathrm{R}^* = \frac{16\sigma^*\mathrm{T}_\infty{}^3}{3\mathrm{k}^*\alpha\rho\mathrm{c}_\mathrm{p}}$ features in the thermal diffusion term in the heat conservation (i.e., $\frac{1}{Pr}(1 + R)\theta''$). The optical and radiative properties of fluid conveying nano-sized particle differ from the thermal properties to either the nanoparticles or the base fluid. Appearance of radiative heat flux dynamize the nanoliquid boundary layer and remarkably increases the magnitudes of temperature because this parameter build ups the thermal diffusion term based on both the flux models (Cattaneo-Christov and Fourier's conduction model). Bég et al. [70] have elaborated that the radiative absorption and thermal

conductivity elevates with temperature in aqueous nanofluid and demotes in non-aqueous nanofluid. Therefor thermal radiation is anticipated as crucial in the coating deposition with nano-polymer. Rosseland model [71] is very realistic approach in multi-physics dynamics and is considerately accurate for large optical thickness affiliated with nanofluids. The present output is in full agreement with Viskanta [72] and Hakeen [73] when the radiative effect is neglected ($R\rightarrow 0$) in processing of materials with high temperature. Thus, the output under-predicts definite temperatures in the coating material. The Rosseland model of diffusion flux is easy which works nicely for dense media (nanofluids) and effectively investigate the impact of radiative heat transfer in the system of coating materials processing. This dispenses a nice stage for extension of present model to P1 differential flux model and surface to surface (STS) radiative flux model [74]. It is further apparent that increasing radiative parameter R, produces an enhancement in nanoparticle concentration. This is also associated with the prescribed convective boundary condition and concentration of nanoparticle on the boundary (wall). Furthermore, it is evident that Powell- Eyring fluid attain significantly lower temperature when compared with Newtonian fluid i. e. substantial cooling of the coating is achieved with rheological properties and this is beneficial to practical operations.

Fig. 7(a) and Fig. 7(b) illustrate the impact of thermal Biot number (γ) on temperature and nanoparticle concentration profiles again for Fourier and Cattaneo-Christov flux models. The non-Fourier model produces lower nanoparticle concentrations and temperatures than classical Fourier model. Thermal and species boundary layer thickness thickness are therefore decreased for the non-Fourier model. For both Powell-Eyring fluid and Newtonian, the temperature is increased with rise in γ and thus is increasing function of Biot number. For both the flux models, there is also a significant increment in temperature with larger value of γ at the boundary surface. Also, in the absence of Biot number effect, the temperature reduces which stipulates that the temperature is under-predicated which can be commentative in polymeric coatings [75].

Fig. 8(a) and Fig. 8(b) explores the influence of Biot number γ on the thermal and nanoparticle concentrations for Newtonian and Powell-Eyring fluid. Regimes with less Biot numbers ($\gamma \ll 1$) are thermally simple and greater value of γ Biot numbers ($\gamma \gg 1$) represents complex regimes due to uniformity and non-uniformity of temperature fields respectively. Higher value of γ results in a boost in temperature and nanoparticle concentration. Further, temperature and nanoparticle concentration due to the flow of Newtonian fluid is more as compared to that of Eyring-Powell fluid. For both Powell-Eyring and Newtonian fluid, thermal and concentration boundary layer are enhanced with rise in Biot number, indicating that the convective wall condition is independent of nanoliquid rheology. Thus, with

increasing impact of the convective condition at boundary, the magnitudes of temperature and nanoparticle concentrations are elevated.

Fig. 9(a) and Fig. 9(b) explore the impact of thermal relaxation parameter on tempearature and nanoparticle concentration in presence or absence of themal radiation (i. e. R=0, indicates the absence of radiation). It is spotted here that temperature without considering radiation is remarkably less than with radiative flux present. A similar pattern is observed for nanoparticle volume fraction i. e. nanoparticle diffusion is enhanced with energization of the coating regime via stronger radiative heat transfer. However, with increasing thermal relaxation parameter leads to depletion in nanoparticle concentration and temperature. Non-Fourier hyperbolic heat conduction produces a cooling in the coating and inhibits nanoparticle migration in the boundary layer. Fourier parabolic heat conduction produces much higher temperatures and nanoparticle concentrations.

Fig. 10 – Fig. 12 visualize the impact of parameters of Eyring-Powell fluid (ε), Prandtl number (Pr), thermophoresis (Nt) and Brownian motion (Nb) on skin coefficient friction, Nusselt and Sherwood number versus ξ. Skin friction coefficient reduces with increment in Eyring-Powell fluid (ε) against mixed convection parameter. Nusselt number (corresponds Rate of heat transfer) is however enhanced with ξ and a rise in Prandtl number. Sherwood number i. e. wall rate of mass transfer against parameter ξ is suppressed with enlarging values of thermophoresis parameter (nanoparticle concentrations in the bulk fluid are increased) and enhanced more with rise in value of Brownian motion parameter (nanoparticle concentrations in the bulk fluid are reduced). It is quite observed that enhancing the Brownian motion parameter results in reduction in the nanoparticle volume fraction (percentage of nano – sized particle in the base fluid). Brownian motion parameter N_b appears in a coupled and species-thermal diffusion part in the Buongiorno model (eqn. (14)). The species diffusion term is diminished when the coupled diffusion term possesses larger value. But the known restriction in Buongiorno model is that the actual types of nano-sized particles (CNTs, metallic oxides, etc.) cannot be simulated because it does not make room for the properties of nanoparticles. This limitation can be attainable by Tiwari-Das model (as explained by Bég et al. [71]) with further limitation that this model eliminates the concentration equation and does not emphasize a mechanism for nanoparticle diffusion. This dilemma is currently under disquisition. Nt replicates the effects of thermophoretic body force. Rise in thermophoretic force enhances the motion of nanoparticles away from the wall and increase the concentration of nanoparticles in the boundary layer regime which results in decrease in rate of mass transfer (Sherwood Number).

Table 3. Effect of various parameters on the $-f''(0,\xi)$, $\theta'(0,\xi)$ and $\phi'(0,\xi)$

δ^*	ε	ξ	Pr	β	R	γ	Nt	Nb	$-f''(0,\xi)$	$\theta'(0,\xi)$	$\phi'(0,\xi)$
0									0.66387	0.48666	0.486658
0.5									0.68233	0.48619	0.486187
1									0.70703	0.48559	0.48559
2									0.80083	0.48396	0.48396
	0								0.91607	0.47461	0.474607
	0.5								0.76292	0.48201	0.482011
	1								0.66726	0.48656	0.486564
	2								0.57161	0.49175	0.491752
	1	0							0.71137	0.48472	0.484721
		1							0.62496	0.48842	0.488423
		2							0.544	0.49664	0.496638
		0.5	1						0.66726	0.48656	0.486564
			2						0.68553	0.55723	0.557229
			5						0.69843	0.63155	0.63155
			1	0					0.66173	0.46812	0.468116
				0.2					0.6718	0.50226	0.50226
				0.5					0.6807	0.53896	0.538957
				0.1	0				0.67904	0.52926	0.529259
					0.5				0.66726	0.48656	0.486564
					1				0.65677	0.45427	0.454271
					0.5	0.1			0.70283	0.0925	0.092505
						0.5			0.67888	0.35627	0.356268
						1			0.66127	0.55421	0.554209
						0.8	0.1		0.66726	0.48656	0.486564
							0.3		0.66701	0.48583	1.457496
							0.5		0.66676	0.4851	2.425492
								0.1	0.66726	0.48656	0.486564
								0.3	0.66726	0.48656	0.162188
								0.5	0.66725	0.48656	0.097313

Finally values for wall gradient functions, $-f''(0,\xi)$, $\theta'(0,\xi)$ and $\phi'(0,\xi)$ for all thermophysical parameters, are displayed in **Table 3**. The condition required for distribution of nanoparticle volume fraction at the wall of the vertical sheet which is enabled via the revised Buongiorno model is appropriately satisfied (i. e. $\mathrm{Nb}\phi'(0,\xi) + \mathrm{Nt}\theta'(0,\xi) = 0$). The skin coefficient friction can be easily derived as we have obtained the value of $f''(0,\xi)$. Further, it is observed that $-f''(0,\xi)$ varies linearly grows with δ^*, Pr and β whereas it shrinks with enhancing ε, ξ, R and γ. Additionally, the Nusselt number is enhanced by Biot number, Prandtl number and reduces as the radiation parameter increases since the fluid conveying nano-sized particle coating is heated with stronger radiative flux and there is a suppression in heat transfer away from the bulk fluid to the wall (plate). Additionally, an increment in Brownian motion manifests in a reduction in rate of nanoparticle mass transfer (Sherwood number) whereas elevation in thermophoresis parameter produces the opposite effect i.e. an increase in Sherwood number.

5.CONCLUSIONS

The current study scrutinizes steady incompressible convective boundary layer flow of kinetic theory-based Eyring-Powell fluid conveying nano-sized particle from a vertical plane surface considering thermal radiation effects. The vertical plate is prescribed a convective boundary condition and a modified distribution of nanoparticles fraction over the surface. The Cattaneo-Christov non-Fourier model is adopted which incorporates thermal relaxation effects for finite wave hyperbolic heat waves. The local non-similarity method and the Liao Homotopy Analysis Method (HAM) are deployed to evaluate the transformed dimensionless two-parameter boundary layer equations with associated wall and free stream conditions. Excellent collaboration of the converged results for both methods are achieved with the existing results. Validation of special cases of the general model is also included with published literature. The variation of heat transfer due to Cattaneo-Christov and Fourier's model is investigated and analysed. The main outcomes of the study are:

- Flow of Eyring-Powell fluid conveying nano-sized particle achieves higher velocities than the Newtonian fluid which is attributable to the pseudoplasticity i. e. shear thinning behaviour.
- Thermal relaxation in the non-Fourier model (hyperbolic) enables the heat transfer process to occur with greater time as compared to the heat transfer by classical Fourier's law (parabolic).
- By raising thermal buoyancy effect, molecular motion of the fluid particles is exacerbated whereas less interaction and less collision between nanoparticles and fluid particles are caused. Thermal and

nanoparticle boundary layer thicknesses are reduced while momentum boundary layer thickness is reduced (flow acceleration) with enhancement in mixed convection parameter.

- Skin coefficient friction exhibits a linear increase with Prandtl number and thermal relaxation (Catteano-Christov) parameter δ^*, Pr and β whereas it is decreasing function of ε,ξ, R and γ. Also, the Nusselt number is enhanced with elevation in Biot number, Prandtl number and decreases as the value of radiation parameter increases.
- Enhancing Brownian motion induces a reduction in mass transfer rates of nanoparticles i. e. Sherwood number while an increment in thermophoresis parameter results in an increment in Sherwood number.

The current study has considered steady state fluid conveying nano-sized particle coating flow and has ignored chemical reactions e.g. homogenous and heterogenous chemical reactions, which are also important in nanocoating manufacturing processes. Future investigations may address time-dependent effects, chemical reactions and furthermore explore alternative non-Newtonian models e.g. micropolar viscoelastic rheological formulations [76], which are also of interest in modelling different characteristics of smart coating transport phenomena. The outputs of these studies will be imminently communicated.

Nomenclature

A_i	Arbitrary Constants ($i = 1, 2, ..., 7$)
c_p	Heat capacity
C_f	Skin friction
D_B	Brownian diffusion coefficient of the species
D_T	Thermophoretic diffusion coefficient of the species
f	Non-dimensional velocity
$f(\eta, \xi)$	Dimensionless velocity function
$f_0(\eta, \xi)$,	Initial guess of $F(\eta, \xi)$
$f^*_m(\eta, \xi)$	Solution of mth order deformation equation for $f(\eta, \xi)$
Gr_x	Local Grashof number
H_i	Auxiliary functions in HAM ($i = 1, 2, 3$)
h_i	Control parameter for F, θ and ($i = 1, 2, 3$)
k	Thermal conductivity of the fluid
k^*	Mean absorption coefficient
L_i	Auxiliary linear operator ($i = 1, 2, 3$)

m_w	Rate of mass transfer
Nb	Brownian motion parameter
Nt	thermophoresis parameter
Nu	Local Nusselt number
N_i	Auxiliary non-linear operator ($i = 1, 2, 3$)
$P(\eta, \xi)$	Auxiliary function of $f(\eta, \xi)$ in terms of derivative of $f(\eta, \xi)$ w.r.t. ξ
p	Embedding parameter
Pr	Prandtl number
q_r	Radiative flux
$Q(\eta, \xi)$	Auxiliary function of $\theta(\eta, \xi)$ in terms of derivative of $\theta(\eta, \xi)$ w.r.t. ξ
q^*_w	Rate of heat transfer
$R(\eta, \xi)$	Auxiliary function of $\phi(\eta, \xi)$ in terms of derivative of $\phi(\eta, \xi)$ w.r.t. ξ
Re_x	Local Reynolds number
R	Radiation parameter
Sc	Schmidt number
Sh	Sherwood number
T	Fluid temperature
T_∞	Ambient fluid (free stream)
u	Translational velocity along the x-direction
v	Translational velocity along the y-direction
x, y	Coordinate axes

Greek Symbols

α	Thermal diffusivity
β	Thermal relaxation parameter
γ	Biot number
ε, δ	Non-Newtonian fluid parameters
ρ	Density
ψ	Dimensionless stream function
$\theta(\eta, \xi)$	Dimensionless temperature function
$\theta_0(\eta, \xi)$	Initial guess of $\theta(\eta, \xi)$
$\theta^*_m(\eta, \xi)$	Solution of mth order deformation equation for $\theta(\eta, \xi)$
$\phi(\eta, \xi)$	Dimensionless concentration function
$\phi_0(\eta, \xi)$	Initial guess of $\phi(\eta, \xi)$
$\phi^*_m(\eta, \xi)$	Solution of mth order deformation equation for $\phi(\eta, \xi)$
η	Pseudo-similarity coordinate in the *y*-direction
μ	dynamic viscosity
τ_x	Local dimensional wall shear stress
σ^*	Stefan Boltzmann constant
ξ, η	Streamwise and transverse coordinates

Subscripts

w	Wall conditions
∞	Ambient condition

Superscripts

'	Prime denotes the derivative with respect to η

Acknowledgements

The authors are thankful to all reviewers for their useful and constructive comments which have helped to improve the present article.

REFERENCES

[1] K. R. Rajagopal, Na, T. Y., Natural convection flow of a non-Newtonian fluid between two vertical flat plates, Acta Mechanica, 54(3-4) (1985) 239-246.
[2] M. Huang, J. Huang, Y. Chou, C. O. Chen, Effects of Prandtl number on free convection heat transfer from a vertical plate to a non-Newtonian fluid. ASME J. Heat Transf., 111(1) (1989).
[3] R. S. R. Gorla, A. Slaouti, H.S. Takhar, Mixed convection in non-Newtonian fluids along a vertical plate in porous media with surface mass transfer, Int. J. Numer. Method H., 7(6) (1997) 598-608.
[4] D. Gupta, L. Kumar, O. A. Bég, B. Singh (2014) Finite element analysis of transient heat and mass transfer in microstructural boundary layer flow from porous stretching sheet. Comput. Therm. Sci. 6(2):155-169.
[5] A. Subba Rao, V. Ramachandra Prasad, N. Bhaskar Reddy, O. Anwar Bég, Heat transfer in a Casson rheological fluid from a semi-infinite vertical plate with partial slip, Heat Transf. Asian Res. 44 (2015) 272-291.
[6] O. Anwar Bég, J. Zueco, S.K. Ghosh Unsteady natural convection of a short-memory viscoelastic fluid in a non-Darcian regime: network simulation, Chem. Eng. Commun., 198, 172-190 (2010).
[7] O. Anwar Bég, O.D. Makinde, Viscoelastic flow and species transfer in a Darcian high-permeability channel, Petroleum Sci. Eng., 76 (2011) 93–99.
[8] A. K. Ray, B. Vasu, P. V. S. N. Murthy, R. S. R. Gorla, Non-similar solution of Eyring–Powell fluid flow and heat transfer with convective boundary condition: homotopy analysis method, Appl. Comput. Math-Bak, 6(1) (2020) 16.
[9] Manghat, R., Mahanthesh, B., & Shehzad, S. A. (2021). Two-phase Sakiadis flow of a nanoliquid with nonlinear Boussinesq approximation and Brownian motion past a vertical plate: Koo-Kleinstreuer-Li model. *Heat Transfer*, *50*(2), 1853-1871.
[10] J. Buongiorno, Convective transport in nanofluids, ASME J. Heat Trans., 128 (2006) 240-250.
[11] K. Swain, B. Mahanthesh, & F. Mebarek-Oudina, Heat transport and stagnation-point flow of magnetized nanoliquid with variable thermal conductivity, Brownian moment, and thermophoresis aspects, Heat Transfer, 50(1) (2021) 754-767.
[12] A.V. Kuznetsov, D.A. Nield, Natural convective boundary-layer flow of a nanofluid past a vertical plate: A revised model. Int. J. Therm. Sci. 77 (2014) 126–129.
[13] P.K. Kameswaran, B. Vasu, P.V.S.N. Murthy, R.S.R. Gorla, Mixed convection from a wavy surface embedded in a thermally stratified nanofluid saturated porous medium with non-linear Boussinesq approximation. Int. Commun. Heat Mass, 77 (2016) 78–86.
[14] A. Malvandi, D. D. Ganji, Brownian motion and thermophoresis effects on slip flow of alumina/water nanofluid inside a circular microchannel in the presence of a magnetic field, Int. J. Therm. Sci. 84 (2014) 196–206.

[15] I. L. Animasaun, R. O. Ibraheem, B. Mahanthesh, H. A. Babatunde, A meta-analysis on the effects of haphazard motion of tiny/nano-sized particles on the dynamics and other physical properties of some fluids. Chin. J. Phys., 60 (2019) 676-687.
[16] A. Wakif, I. L. Animasaun, P. S. Narayana, G. Sarojamma, Meta-analysis on thermo-migration of tiny/nano-sized particles in the motion of various fluids. Chin. J. Phys. 68 (2020) 293-307.
[17] A. K. Ray, B. Vasu, O. A. Bég, R. S. R. Gorla, P. V. S. N. Murthy, Homotopy semi-numerical modeling of non-Newtonian nanofluid transport external to multiple geometries using a revised Buongiorno Model. Inventions, 4(4) (2019) 54.
[18] B. Vasu, A. Dubey, O. Anwar Bég, Finite element analysis of non-Newtonian magneto-hemodynamic flow conveying nanoparticles through a stenosed coronary artery, Heat Transf. Asian Res., 47 (2019) 1-34.
[19] J. B. J. Fourier, Theorie Analytique de la Chaleur. Paris: Chez Firmin Didot, 1822.
[20] C. Cattaneo, Sulla conduzionedelcalore. Attisemin Mat Fis Univ Modena Reggio Emilia, 3:17 (1948) 83–101.
[21] C. I. Christov, On frame indifferent formulation of the Maxwell–Cattaneo model of finite-speed heat conduction. Mech. Res. Commun. 36 (2009) 481–486.
[22] A. Shahid, M. M. Bhatti, O. Anwar Bég, A. Kadir, Numerical study of radiative Maxwell viscoelastic magnetized flow from a stretching permeable sheet with the Cattaneo–Christov heat flux model, Neural Comput. Appl. 30(11) (2018) 3467-3478.
[23] A. Sarkar, P. K. Kundu, Exploring the Cattaneo-Christov heat flux phenomenon on a Maxwell-type nanofluid coexisting with homogeneous/heterogeneous reactions. Eur. Phys. J. Plus, 132(12) (2017) 534.
[24] B. Vasu, C. RamReddy, P. V. S. N. Murthy, R. S. R. Gorla, Entropy generation analysis in nonlinear convection flow of thermally stratified fluid in saturated porous medium with convective boundary condition, ASME J. Heat Transf., 139(9) (2017) 091701 (10 Pages).
[25] N. S. Akbar, O. Anwar Bég, Z. H. Khan, Magneto-nanofluid flow with heat transfer past a stretching surface with a new heat flux model using numerical approach. Int J Numer. Methods H., 27(6) (2017)1-17.
[26] B. Vasu, A. K. Ray, R. S. R. Gorla, Free convective heat transfer in Jeffrey fluid with suspended nanoparticles and Cattaneo–Christov heat flux, Proceedings of the Institution of Mechanical Engineers, Part N: Journal of Nanomaterials, Nanoengineering and Nanosystems, 2397791420912628, (2020).
[27] R. Mehmood, S. Rana, O. Anwar Bég and A. Kadir, Numerical study of chemical reaction effects in magnetohydrodynamic Oldroyd-B oblique stagnation flow with a non-Fourier heat flux model, J. Brazilian Soc. Mech Sci. Eng. 40 (11) (2018) 526.
[28] B. Vasu, A. K. Ray, Numerical study of Carreau nanofluid flow past vertical plate with the Cattaneo–Christov heat flux model, Int. J. Numer. Method H., 29 (2) (2019) 702-723.
[29] F Irgens, Rheology and non-Newtonian Fluids. Springer International Publishing, (2014)
[30] R.P. Chhabra, J. Richardson, Non-Newtonian Flow and Applied Rheology: Engineering Applications, 2nd ed.; Butterworth-Heinemann: Oxford, UK, (2008)
[31] B. Vasu, R. S. R. Gorla, P. V. S. N. Murthy, Thermophoresis on boundary layer heat and mass transfer flow of Walters – B fluid past a radiate plate with heat sink/ source, Heat Mass Transf., 52 (2016) 10.
[32] A. K. Ray, B. Vasu, Hydrodynamics of non-Newtonian Spriggs fluid flow past an impulsively moving plate, Applications of Fluid Dynamics, Springer, Singapore, (2018) 95-107.
[33] A. Dubey, B. Vasu, O. A. Bég, R. S. R. Gorla, A. Kadir, Computational fluid dynamic simulation of two-fluid non-Newtonian nanohemodynamics through a diseased artery with a stenosis and aneurysm. Comput Method Biomech. Biomed. Eng., (2020) 1-27.
[34] N. Ali, A. Zaman, O. A. Bég, T. Hayat, Mathematical model for isothermal wire-coating from a bath of Giesekus viscoelastic fluid, Chem. Eng. Comm. 203, 1336-1248 (2016).

[35] N. Manzoor, O. A. Bég, K. Maqbool and S. Shaheen, Mathematical modelling of ciliary propulsion of an electrically-conducting Johnson-Segalman physiological fluid in a channel with slip, Computer Methods in Biomechanics and Biomedical Engineering (2019). https://doi.org/10.1080/10255842.2019.1582033

[36] H. Thameem Basha, R. Sivaraj, V. R. Prasad, O. Anwar Bég, Entropy generation of tangent hyperbolic nanofluid flow over a circular cylinder in the presence of nonlinear Boussinesq approximation: A non-similar solution, J. Thermal Analysis and Calorimetry (2020). https://doi.org/10.1007/s10973-020-09981-5

[37] A. Kumar, R. Tripathi, R. Singh, V. K. Chaurasiya, Simultaneous effects of nonlinear thermal radiation and Joule heating on the flow of Williamson nanofluid with entropy generation, Phys. A: Stat. Mech. Appl., 551 (2020) 123972.

[38] M. Norouzi. S. Z. Daghighi. O. Anwar Bég, Exact analysis of heat convection of viscoelastic FENE-P fluids through isothermal slits and tubes, Meccanica, 53 (2018) 817-831.

[39] H. Basha, G. Janardhana Reddy, N. S. Venkata Narayanan and O. Anwar Bég, Supercritical heat transfer characteristics of couple stress convection flow from a vertical cylinder using an equation of state approach, J. Molecular Liquids, 277 (2019) 434-452.

[40] A.Subbarao, V.R. Prasad, V. Naga Radhika and O. Anwar Bég, Heat transfer in viscoplastic boundary layer flow from a vertical permeable cone with momentum and thermal wall slip: numerical study, Heat Transf. Res., 49(3) (2018) 189–204.

[41] R.E. Powell, H. Eyring, Mechanisms for the relaxation theory of viscosity. Nature 154 (1944) 427–428.

[42] I. L. Animasaun, O. K. Koriko, K. S. Adegbie, H. A. Babatunde, R. O. Ibraheem, N. Sandeep, B. Mahanthesh, Comparative analysis between 36 nm and 47 nm alumina–water nanofluid flows in the presence of Hall effect. J. Therm. Anal. Calorim. 135(2) (2019), 873-886.

[43] O. A. Abegunrin, I. L. Animasaun, N. Sandeep, Insight into the boundary layer flow of non-Newtonian Eyring-Powell fluid due to catalytic surface reaction on an upper horizontal surface of a paraboloid of revolution. Alexandria engineering journal, 57(3) (2018) 2051-2060.

[44] G. Kumaran, R. Sivaraj, V. Ramachandra Prasad, O. Anwar Bég and R. Prakash Sharma, Finite difference computation of free magneto-convective Powell-Eyring nanofluid flow over a permeable cylinder with variable thermal conductivity, Physica Scripta, 96 (2021) 025222, 1-30.

[45] S. A. Gaffar, V. R. Prasad, B. Vijaya and O. Anwar Bég, Mixed convection flow of magnetic viscoelastic polymer from a non-isothermal wedge with Biot number effects, Int. J. Eng. Math., 2015, Article ID 287623, 15 pages (2015).

[46] I. L. Animasaun, B. Mahanthesh, O. K. Koriko, On the motion of non-Newtonian Eyring–Powell fluid conveying tiny gold particles due to generalized surface slip velocity and buoyancy. International Journal of Applied and Computational Mathematics, 4(6) (2018) 1-22.

[47] E.M. Sparrow, H.S. Yu, Local non-similarity thermal boundary layer solutions. ASME J Heat Transf., 93 (1971) 328–334.

[48] W. J. Minkowycz, E. M. Sparrow, Numerical solution scheme for local non-similarity boundary layer analysis. Numer Heat Transfer, 1, (1978) 69–85.

[49] M. Massoudi, Local non-similarity solutions for the flow of a non-Newtonian fluid over a wedge. Int. J. Nonlin. Mech, 36(6) 2001 961–976.

[50] O. Anwar Bég, A. Bakier, V.R. Prasad and S. K. Ghosh, Numerical modelling of non-similar mixed convection heat and species transfer along an inclined solar energy collector surface with cross diffusion effects, World Journal of Mechanics, 1, 185-196 (2011).

[51] O. Anwar Bég, Bakier, A.Y. and V.R. Prasad, Numerical study of free convection magnetohydrodynamic heat and mass transfer from a stretching surface to a saturated porous medium with Soret and Dufour effects, Computational Materials Science, 46, 1, 57-65 (2009).

[52] M. Mushtaq, S. Asghar, M. A. Hossain, Mixed convection flow of second grade fluid along a vertical stretching flat surface with variable surface temperature, Heat Mass Transf., 43(10) (2007) 1049.
[53] N.C. Roy, M.A. Hossain, Numerical solution of a steady natural convection flow from a vertical plate with the combined effects of streamwise temperature and species concentration variations. Heat Mass Transf., 46 (2010) 509–522.
[54] A.J. Chamkha, A.M. Rashad, R.S.R. Gorla, Non-similar solutions for mixed convection along a wedge embedded in a porous medium saturated by a non-Newtonian nanofluid: natural convection dominated regime. Int. J. Num. Method H., 24(7) (2014) 1471–1486.
[55] S. Liao, Beyond Peturbation: An Introduction to the Homotopy Analysis Method, CRC Press, Florida, USA (2011).
[56] B. Vasu, A. K. Ray, O. A. Bég and R. S. R. Gorla, Magneto-bioconvection flow of a Casson thin film with nanoparticles over an unsteady stretching sheet: HAM and GDQ computation, Int. J. Numer. Method H., 29 (11) (2019) 4277-4309.
[57] D. Tripathi and O. Anwar Bég, Peristaltic transport of Maxwell viscoelastic fluids with a slip condition: Homotopy analysis of gastric transport, J. Mech Med Biology, 15 (3) (2015) 1550021.42
[58] A. K. Ray, B. Vasu, R. S. R. Gorla, Homotopy simulation of non-Newtonian Spriggs fluid flow over a flat plate with oscillating motion, Int. J. Appl. Mech., 24 (2) (2019) 359-385.
[59] N. Shukla, P. Rana, O. A. Bég, B. Singh, A. Kadir, Homotopy study of magnetohydrodynamic mixed convection nanofluid multiple slip flow and heat transfer from a vertical cylinder with entropy generation, Propuls. Power Res. 8(2) (2019) 147-162.
[60] A. K. Ray, B. Vasu, Influence of chemically radiative nanoparticles on flow of Maxwell electrically conducting fluid over a convectively heated exponential stretching sheet. World J. Eng., 16(6) (2019) 791-805.
[61] O. Anwar Bég, F. Mabood and M. Nazrul Islam, Homotopy simulation of nonlinear unsteady rotating nanofluid flow from a spinning body, Int. J. Eng. Math., 2015, (2015) 1-15.
[62] J. Srinivas and O. Anwar Bég, Homotopy study of entropy generation in magnetized micropolar flow in a vertical parallel plate channel with buoyancy effect, Heat Transf. Res., 49(6): 529–553 (2018).
[63] O. A. Bég, B. Vasu, A. K. Ray, T.A. Bég, Ali Kadir, Henry J. Leonard and R.S.R. Gorla, Homotopy simulation of dissipative micropolar flow and heat transfer from a two-dimensional body with heat sink effect: applications in polymer coating, Chem. Biochem. Eng. Q. (2021). **In Press**
[64] O. Anwar Bég, S. Jangili, Tasveer A. Bég, M. Shankar Rao, Homotopy analysis of Maxwell displacement current and oblique magnetic field effects on unsteady rotating duct flow of partially ionized dielectric hydrogen gas, Int. J. Hydrogen Energy (2021). **In Press**
[65] H. Benkreira, M. F. Edwards, W. L. Wilkinson, A semi-empirical model of the forward roll coating flow of Newtonian fluids. Chem. Eng. Sci. 36(2) (1981) 423-427.
[66] Coyle, D. Liquid Film Coating (eds S. F. Kistler and P. M. Schweizer). Chapman and Hall, Ch. 12a (1996).
[67] J. R. Pearson, Mechanics of Polymer Processing. London and New York: Elsevier Applied Science Publications (1985).
[68] H. M. Thompson, A theoretical investigation of roll coating phenomena, PhD thesis, University of Leeds, UK (1992).
[69] P. H. Gaskell, M. D. Savage, J. L. Summers, H. M. Thompson, Flow topology and transformation in fixed gap symmetric forward roll coating systems. Proc. 9th Int. Conf. Num. Meth. Lam. and Turb. Flow, (1995) 984-995.
[71] O. A. Bég, S. Kuharat, M. Ferdows, M. Das, A. Kadir, M. Shamshuddin, Magnetic nano-polymer flow with magnetic induction and nanoparticle solid volume fraction effects: solar magnetic nano-polymer fabrication simulation, Proc. IMechE-Part N: J Nanomaterial Nanoengineering and Nano-systems 233(1) (2019) 27-45.

[72] R. Viskanta R., Radiation heat transfer in materials processing and manufacturing, Energy Environ., 15 (1999) 101-112.
[73] A. K. Hakeem, N. V. Ganesh, B. Ganga, Magnetic field effect on second order slip flow of nanofluid over a stretching/shrinking sheet with thermal radiation effect. J. Magn. Magn. Mater., 381 (2015) 243-257.
[74] S. Kuharat, O. Anwar Bég, A. Kadir and M. Shamshuddin, Computational study of heat transfer in solar collectors with different radiative flux models, Heat Transf. Asian Res., 48 (3) (2019) 1002-1031.
[75] A. Aly, Heat treatment of polymers: a review, Int. J. Mater. Chem. and Phys., 1(2) (2015) 132-140.
[76] K. Madhavi, V.R. Prasad, A. SubbaRao, O. Anwar Bég, A. Kadir, Numerical study of viscoelastic micropolar heat transfer from a vertical cone for thermal polymer coating, Nonlinear Eng., 8(1) (2018) 449-460.